PETROLOGIC INSIGHTS INTO RIFT ZONE MAGMATIC INTERACTIONS

UNDER KĪLAUEA'S NĀPAU CRATER (1922-2011)

A THESIS SUBMITTED TO THE GRADUATE DIVISION OF THE
UNIVERSITY OF HAWAIʻI AT MĀNOA IN PARTIAL FULFILLMENT
OF THE REQUIREMENTS FOR THE DEGREE OF

MASTER OF SCIENCE

IN

GEOLOGY AND GEOPHYSICS

AUGUST 2017

By

Brett Halsey Walker

Thesis Committee:
Michael O. Garcia, Chairperson
Julia E. Hammer
Tim R. Orr

Key words: crystal fractionation; fissure eruption; Kīlauea Volcano; magma mixing; rift zone

DEDICATION

This thesis is in memory of my little bro Dakota Haenel.

(Sept. 30th 1993- May 6th 2015)

The eternal mystery of the world is its comprehensibility...
The fact that it is comprehensible is a miracle.
- Albert Einstein

To learn, you must love discipline;
it is stupid to hate correction.
Proverbs 12:1 (NLT)

ACKNOWLEDGEMENTS

The most influential person who helped this thesis come to fruition is my advisor and mentor, Mike Garcia. I am deeply thankful to him for introducing me to the wonders and frustrations of scientific research. The depth to which he forces me to think about an idea during our discussions has greatly improved my critical thinking and science communication skills.

I am also indebted to my committee members Julia Hammer and Tim Orr, who have been truly gracious and generous with their time during the development of this work. Discussions with them have been invaluable to me. Every time I speak with Julia, I learn something new. Her insightful comments and feedback are always very helpful to me. Likewise, Tim's field experience and proficient knowledge of the locations of eruptive fissures on Kīlauea's East Rift Zone was a huge asset that streamlined our sample collection mission.

This study would not have been possible without the dedicated sampling efforts during the March 2011 Kamoamoa eruption by current and former Hawaiian Volcano Observatory (HVO) staff members. I am thankful to HVO and Hawai'i Volcanoes National Park (HVNP) for permitting the conduction of this research in the Nāpau Crater area and for Tina Neal, who generously provided housing when I arrived at HVNP.

Much of the essential field gear and foul weather outerwear I had the privilege of using during field work was kindly lent to me by Bruce Houghton. I am also grateful to Eileen Chen for assistance in preparing powders and glasses, Michael Rhodes and Michael Vollinger for XRF data, Brian Shiro for episode 59 earthquake data, Tom Shea for sharing his Kīlauea maps, and David Okita for helicopter transport to Nāpau Crater. I thank Kendra Lynn for assistance with fieldwork, microprobe set-up, and olivine diffusion modeling. I recognize Eric Hellebrand for patiently teaching me how to operate the electron microprobe and for his valuable advice on probe work throughout this project.

I am greatly appreciative of my colleagues in the Department of Geology & Geophysics, who have taught me so much about Hawaiian culture and geology along the way. Finally, I sincerely thank my family and friends for their unending love and support. A special thanks goes to my husband, Bernardo Gonzalez, whose jovial character and steadfast encouragement helped me to achieve my goals enthusiastically.

This work was financially supported by the National Science Foundation, grant number EAR-1449744.

ABSTRACT

The high frequency of historical eruptions at Kīlauea Volcano presents an exceptional opportunity to address fundamental questions related to the transport, storage, and interaction of magmas within rift zones. In particular, the Nāpau Crater area on Kīlauea's East Rift Zone (ERZ) has experienced frequent historical fissure eruptions (nine within 50 years). Repeated intrusion and eruption in this region suggests that the Nāpau Crater area serves as a magma mixing 'depot' within the ERZ. Chemical analyses of lavas from fissure eruptions near Nāpau Crater in 1983, 1997, and 2011 have been interpreted to represent mixing between rift-zone-stored magmas and new, summit-derived magma (e.g., Garcia *et al.*, 1992; Thornber *et al.*, 2003; Orr *et al.*, 2015). To better understand potential mixing processes within the ERZ, whole-rock, glass, and mineral compositions were determined for a newly collected suite of samples from the 1963, 1965, 1968, 1983, 1997, and 2011 eruptions. These data help elucidate the pre-eruptive history and temporal evolution of lavas from the most recent eruptive activity near Nāpau Crater in March 2011 (Puʻu ʻŌʻō episode 59). Whole-rock XRF data reveal two geochemically distinct magma batches for the 2011 eruption: one less evolved (6.5-6.6 wt. % MgO) than the other (6.1-6.3 wt. % MgO). Olivine crystals from both batches show normal and reverse zoning, indicating mixing prior to episode 59. Least squares regression calculations document the possibility of mixing between summit-derived magma and residual magma from the 1983 and 1997 eruptions, but surprisingly, show no indication of involvement of earlier magmas from the 1960s. Two physically and chemically distinct pods of stored magma interacted with the episode 59 dike to create the compositions seen in whole-rock analyses of episode 59 lavas. Like the two batches of eruptive products, one storage pod is geochemically more evolved than the other. Least squares regression calculations are consistent with the less evolved pod having contained a fractionated equivalent of 1983 lava and the more evolved pod having contained a hybrid of compositions similar to 1983 and 1997 lavas. Both pods reside at depths ranging from 1.6 to 3.0 km under the Nāpau Crater area. These results clarify the spatial and chemical relations of stored magmas in one of the most frequently active portions of the ERZ and provide insight into their fractionation and mixing histories.

TABLE OF CONTENTS

LIST OF TABLES

Table **Page**

LIST OF FIGURES

LIST OF APPENDICES

INTRODUCTION

Basaltic fissure eruptions are the most common type of volcanic eruptions on Earth (Siebert *et al.*, 2015). On Hawaiian shield volcanoes, fissure eruptions are common along rift zones, which play an integral role in accommodating the magmatic budget (e.g., Dzurisin *et al.*, 1984, Poland *et al.*, 2012). Kīlauea, which composes the southeastern portion of the Island of Hawai‘i (Fig. 1), is one of the most active and intensely studied shield volcano in the world (Tilling & Dvorak, 1993). This ocean island hot-spot volcano has a summit crater and two rift zones that extend east and southwest from the summit caldera. Kīlauea's East Rift Zone (ERZ; Fig. 1) has hosted most of the eruptive activity at Kīlauea since the onset of the Pu‘u ‘Ō‘ō eruption in 1983 (Orr *et al.*, 2015), discharging about 4.4 km^3 of lava as of the end of 2016 (dense-rock equivalent; unpublished data, USGS Hawaiian Volcano Observatory). Lava output at Pu‘u ‘Ō‘ō (Fig. 1) is sustained via a horizontal conduit at ~3 km depth that connects Pu‘u ‘Ō‘ō and the summit (e.g., Klein *et al.*, 1987; Lundgren *et al.*, 2013). The ERZ's magmatic plumbing system can become over-pressurized when magma supply is not accommodated by output at the Pu‘u ‘Ō‘ō vent, leading to fissure eruptions elsewhere along the axis of the ERZ (Heliker & Mattox, 2003; Lundgren *et al.*, 2013). When such a fissure eruption occurs, magma is diverted from the main rift conduit and thus can interact with stored magmas—the vestiges of older intrusions—within the rift zone. The spatial continuity and compositions (and how those change over time) of stored magmas within the ERZ are poorly known. However, much can be learned from petrologic and geochemical investigations on the lavas erupted after a mixing event between rift-conduit dike magma and stored magma.

Petrologic insights gained from research on the lavas produced during significant changes to the magmatic system during a sustained eruption are important for assessing a volcano's magmatic behavior, which plays a role in evaluating its potential future activity. The Pu‘u ‘Ō‘ō eruption, Kīlauea's first multi-decadal flank eruption in more than half a millennium (Orr *et al.*, 2015), provides an opportunity to study the nature of magmatic storage and intrusion within the ERZ. The Nāpau Crater area, located on the middle ERZ (Fig. 1), has experienced more historical fissure eruptions (nine within 50 years; Fig. 2) than any other location on the ERZ. Repeated intrusion and eruption in this region has likely resulted in isolated pods of stored magma that cause the Nāpau Crater area to act as a magma mixing 'depot' within the ERZ,

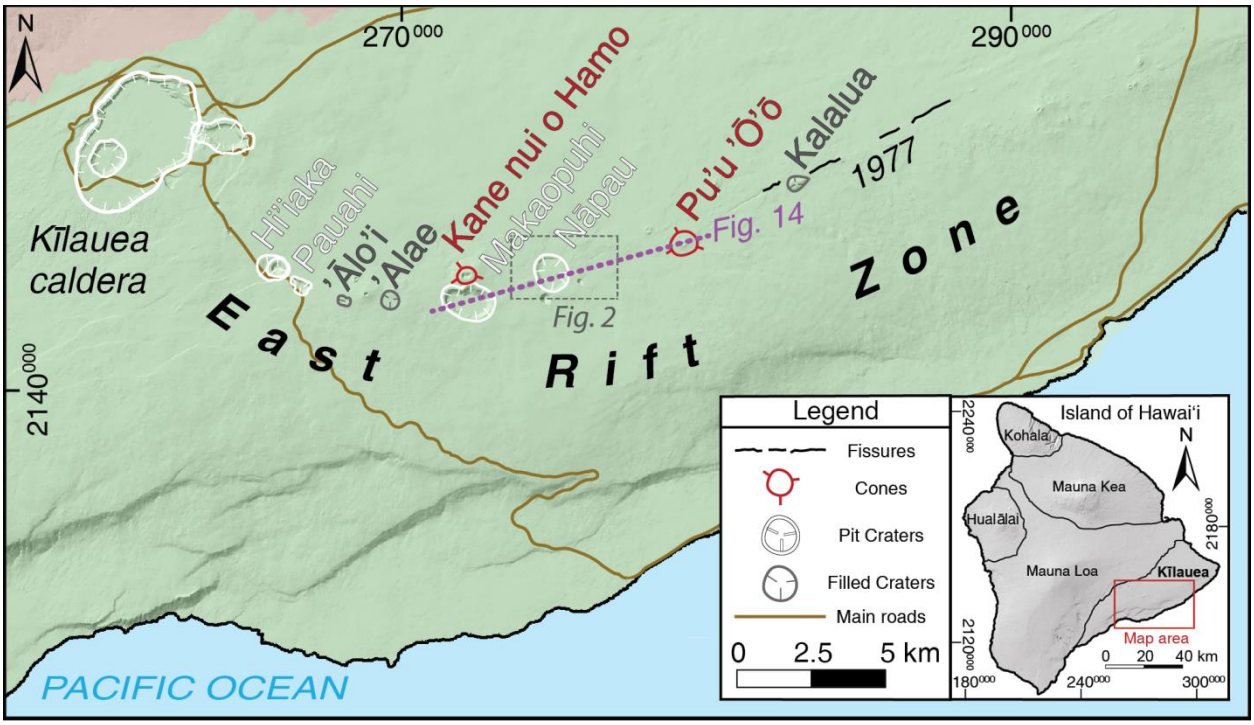

Fig. 1. Map of Kīlauea Volcano's summit region and upper to middle East Rift Zone (ERZ) located on the Island of Hawai'i. The upper ERZ extends from just east of the caldera area downrift along the chain of pit craters to an area approximately between Makaopuhi Crater and Nāpau Crater. From this point to the eastern extension of the map is considered the middle ERZ. Inset map shows location of map (red rectangle) and outlines of the five volcanoes on Hawai'i. Mauna Loa is depicted by the light reddish-brown color in northwestern portion of map. Cross-sectional area of Fig. 14 is represented by the purple dashed line. Fissures of the September 1977 eruption (Moore *et al.*, 1980) are shown because magma from this eruption may have been involved in the March 2011 eruption, despite their location ~7.3 km outside of the Nāpau Crater area (depicted in Fig. 2 and outlined by grey dashed rectangle.) Sources: Geological Maps of Hawaii, Sherrod *et al.* (2007); Digital elevation model (USGS, 2000); coordinate system: UTM Zone 5 (NAD1983).

meaning it is a repository location for several magma storage pods. This area's most recent event, episode 59 of the ongoing Pu'u 'Ō'ō eruption, occurred in March 2011 and is also referred to as the 'Kamoamoa' eruption because it occurred geographically within the Kamoamoa Hawaiian land division. The excellent spatial and temporal coverage of samples collected during episode 59 offer the chance to examine if and how its magma interacted with intrusions from previous Nāpau Crater area eruptions.

Lavas from the upper to middle ERZ (Fig. 1) that erupted in 1963, 1965, 1968, 1969, 1977, 1983 (Pu'u 'Ō'ō episode 1), 1997 (Pu'u 'Ō'ō episode 54), and 2011 (Pu'u 'Ō'ō episode 59) were collected to better understand crustal processes and compositions of stored magma

under the Nāpau Crater area. Whole-rock, glass, and mineral compositions were used to assess the pre-eruptive history of the episode 59 lavas. Olivine crystals from both batches show normal and reverse compositional zoning, which is evidence for magma mixing prior to episode 59. Whole-rock XRF data reveal two geochemically distinct magma batches for episode 59. Least squares regression calculations are consistent with mixing between rift-conduit magma and two different pods of stored magma beneath the Nāpau Crater area. Depending on the proportion of dike magma that mixed with each pod of stored magma during episode 59, the lava erupted either belonged to a more evolved or less evolved batch (Appendix A). The results herein clarify the spatial and chemical relations of stored magmas in one of the most frequently active portions of the ERZ and provide insight into their fractionation and mixing histories.

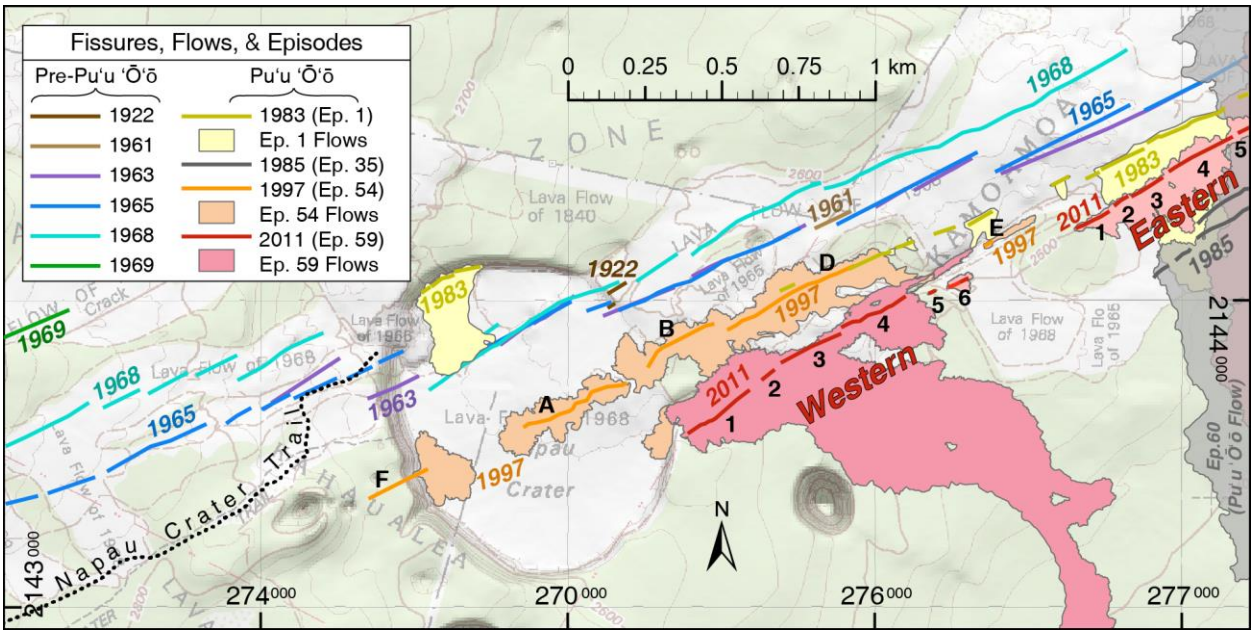

Fig. 2. Map of historical fissure eruptions in the Nāpau Crater area on Kīlauea's middle ERZ. Map area outlined in Fig. 1. Flows from the pre-Pu'u 'Ō'ō fissure eruptions are not shown. Fissures and flows from Pu'u 'Ō'ō eruptions are shown: episode 1 (yellow), episode 35 (non-eruptive fissures; grey), episode 54 (orange), episode 59 (the 'Kamoamoa' eruption; red), and episode 60 (lavas from August 2011; transparent grey). The western Kamoamoa fissure system comprises fissures W-1 to W-6; the eastern system includes fissures E-1 to E-5. Some pre-Pu'u 'Ō'ō fissures are partially (1963, 1965, and 1968) or fully (1961) covered. Outlines of fissure locations and flow fields from T. Orr (pers. com.) and Orr *et al.* (2015). Digital elevation model (USGS, 2000). Coordinate system: UTM Zone 5 (NAD1983).

GEOLOGIC SETTING OF THE NĀPAU CRATER AREA

The Nāpau Crater area on Kīlauea's middle ERZ has experienced ten *en echelon* fissure eruptions within the past century (1922, 1961, 1963, 1965, 1968, 1969, 1983, 1985, 1997, and 2011; Fig. 2). The earlier eruptions (1922-1969) occurred as isolated outbreaks whereas those in 1983 (episode 1), 1985 (episode 35), 1997 (episode 54) and 2011 (episode 59) were part of the ongoing Pu'u 'Ō'ō eruption, which is focused ~4 km downrift from Nāpau Crater (Fig. 1). Many of the eruptions began with seismic swarms that started in the summit area or upper ERZ and propagated downrift to the Nāpau Crater area (e.g., Moore & Koyanagi, 1969; Wright *et al.*, 1968; Swanson *et al.*, 1976). The earthquake swarms related to the 1963, 1968, 1969, 1983, 1997, and 2011 eruptions are thought to have been accompanied by the intrusion of a shallow (~3 km) dike. The historical Nāpau eruptions were of variable duration (0.9-20 days), length of discontinuous eruptive fissure system (2.4-19.2 km), and area covered by new lava (0.1-7.1 km^2; Table 1). The high frequency of historical eruptions in the Nāpau Crater area (most of any area on Kīlauea outside of the summit) and overlapping areas of the ERZ covered by eruptive fissures (Fig. 2) indicate that this section of the rift is underlain by pockets of magma where interactions are likely to occur with new dikes propagating downrift from the upper ERZ.

Historical Pre-Pu'u 'Ō'ō Fissure Eruptions (1922-1977)

1922

The May 1922 eruption formed a lava pond in Makaopuhi Crater and a small spatter rampart and flow on Nāpau Crater's northeastern rim (Jaggar, 1922). Only a few sections of the 1922 spatter rampart remain exposed. This thesis reports the first petrographic and geochemical analyses of samples from the 1922 fissure eruption. Due to the small size of the 1922 outcrop on Nāpau Crater's northeastern rim (~90 m long), only two samples were collected and analyzed. Data associated with these samples will be included in Tables 1, 2, 3, 4, A2, and A4, but these results will not be discussed as a likely mixing component for episode 59 magmas. Residual magma from the 1922 eruption is likely to have been either (1) solidified and unavailable for mixing or, (2) unrecognizably diluted by the subsequent intrusions and eruptions near the exposed 1922 spatter rampart.

Table 1: Key features of historical fissure eruptions in the upper to middle ERZ region.

Date	Key physical features of fissure eruption	MgO range[+] [wt. %]
May 1922	Followed large caldera collapse; summit lava lake drained ≥300 m. Created lava pond in MC and spatter cone on rim of NC. [1]	5.4-6.7[16] ($\bar{x}$ = 6.0)
Sep. 1961	Followed three summit eruptions that occurred earlier in the year. Preceded by earthquake swarm at NC and rapid summit deflation.[2]	6.8-8.6[2] ($\bar{x}$ = 7.7)
Oct. 1963	Summit earthquakes and deflation accompanied seismicity at NC before outbreak. Eruption created lava pond at NC.[3]	6.4-7.7[3] ($\bar{x}$ = 7.3)
Mar. 1965	Summit inflation/collapse transpired. Earthquake swarm near MC prior to eruption, which made lava ponds at NC and MC.[4]	6.8-8.5[4] ($\bar{x}$ = 7.9)
Oct. 1968	Followed previous month's summit eruption. Created lava pond in NC. Seismic patterns implied magma reservoir beneath MC. [5]	6.7-8.2[5] ($\bar{x}$ = 7.3)
Feb. 1969	Summit inflation and upper ERZ earthquakes preceded eruption, which formed a lava pond in ʻĀloʻi Crater.[6]	8.0-9.1[6] ($\bar{x}$ = 8.3)
Sep. 1977	Rapid summit deflation (without inflation) and seismic activity near MC shifted eastward to KC, where eruption ensued.[7]	5.3-5.9[7] ($\bar{x}$ = 5.6)
Jan. 1983	Episode 1 of Puʻu ʻŌʻō. [8] Magma reservoir under Nāpau Crater hypothesized based on seismic/geodetic patterns.[9]	5.7-6.6[10] ($\bar{x}$ = 6.1)
July. 1985	Episode 35 of Puʻu ʻŌʻō. Intrusion uprift from shallow Puʻu ʻŌʻō storage reservoir into Kamoamoa area.	7.6-7.9[11] ($\bar{x}$ = 7.8)
Jan. 1997	Episode 54 of Puʻu ʻŌʻō. Puʻu ʻŌʻō lava lake drained[12], seismicity at summit and NC during and after eruption.[13]	5.6-6.4[14] ($\bar{x}$ = 6.2)
Mar. 2011	Episode 59 of Puʻu ʻŌʻō. Followed summit and Puʻu ʻŌʻō inflation caused by magmatic overpressure. [15]	6.1-6.6[16] ($\bar{x}$ = 6.3)

Notes: Abbreviations: MC (Makaopuhi Crater), NC (Nāpau Crater), KC (Kalalua Crater), $\bar{x}$ (sample mean). [+]MgO ranges are whole-rock values. Sources: (Jaggar, 1922)[1]; (Richter *et al.*, 1964)[2]; (Moore & Koyanagi, 1969)[3]; (Wright *et al.*, 1968)[4]; (Jackson *et al.*, 1975)[5]; (Swanson *et al.*, 1976)[6]; (Moore *et al.*, 1980)[7]; (Wolfe *et al.*, 1988)[8]; (Okamura *et al.*, 1988) [9], (Garcia *et al.*, 1989)[10]; (Thornber *et al.* (2002)[11]; (Harris *et al.*, 1997)[12]; (Thornber *et al.*, 2003)[13]; (Garcia *et al.*, 2000)[14]; (Orr *et al.*, 2015)[15]; (this study)[16].

1961

An earthquake swarm and strong harmonic tremor near Nāpau Crater was accompanied by rapid summit detumescence preceding the September 1961 eruption, which produced the longest historical fissure system on the ERZ since 1840 (Fig. 3d; Richter *et al.*, 1964). The flows from this eruption in the Nāpau Crater area are buried.

1963

Detumescence and earthquakes at the summit along with strong harmonic tremor and earthquakes at Nāpau Crater preceded the October 1963 outbreak (Moore & Koyanagi, 1969). During this eruption, a 7-m-deep lava pond formed in Nāpau Crater and eruptive fissures extended downrift from just west of Nāpau Crater to 3 km beyond Kalalua Crater (Fig. 1; Moore & Koyanagi, 1969).

1965

The March 1965 eruption was preceded by inflation at the summit and accompanied by a summit collapse (Wright *et al.*, 1968). Earthquake swarms in Kīlauea's caldera and Makaopuhi Crater began ~1 hour before the eruption (Wright *et al.*, 1968). The resulting lava covered more area than any other historical Nāpau Crater area eruption between 1840 and 1983 (7.1 km^2; Fig. 3a). The 1965 eruption also produced lava ponds in Makaopuhi Crater (83 m deep) and Nāpau Crater (12 m deep), and its fissure system extended downrift from Makaopuhi Crater nearly to Kalalua Crater (Wright *et al.*, 1968; Fig. 3d). In the Nāpau Crater area, the 1965 fissures are adjacent to (≤60 m) the 1963 fissures (Fig. 2).

1968

The vents of the October 1968 eruption are located along a series of fissures that pass through Nāpau Crater and extend downrift past the east flank of Kane Nui o Hamo (Jackson *et al.*, 1975; Fig. 3d; Fig. 1). These fissures are 0-200 m north of the March 1965 fissures (Fig. 2) and were preceded and accompanied by shallow earthquakes as magma worked its way to the surface (Jackson *et al.*, 1975). No earthquakes occurred between the summit and ʻAlae Crater (Fig. 1) during the October 1968 eruption. The seismic patterns during the 4 hours preceding this eruption indicated a forceful injection of magma by hydraulic fracturing under the Makaopuhi Crater area. This suggested the presence of a shallow magma reservoir in the Makaopuhi Crater area before the eruption (Jackson *et al.*, 1975).

1969

The February 1969 eruption began 6.6 km uprift of Nāpau Crater (Swanson *et al.*, 1976) and its fissures are offset 300-400 m north along the trend of the 1968 vents (Fig. 2). Like the October 1968 eruption, the February 1969 eruption lacked earthquakes between the summit and eruption area before and during the eruption (Swanson *et al.*, 1976). These seismic data support the interpretation that feeder dikes intruded upward from the main magmatic conduit within the ERZ, which is connected to the summit reservoir (Swanson *et al.*, 1976).

1977

Seismic evidence related to the September 1977 eruption demonstrates that magma was injected into the ERZ from the summit region via a conduit that passed underneath Nāpau Crater (Moore *et al.*, 1980). Seismic activity in the upper ERZ increased and peaked near Makaopuhi Crater prior to this eruption without any significant summit inflation (Moore *et al.*, 1980). On the day

before the eruption, the summit rapidly deflated and an earthquake swarm migrated from Makaopuhi Crater downrift past Nāpau Crater, localizing near Kalalua Crater (Moore *et al.*, 1980). Although the 1977 eruption took place ~7.3 km downrift of Nāpau Crater, lavas from this eruption were evaluated as a potential mixing component in episode 59 lavas because of their inferred involvement in the Puʻu ʻŌʻō episode 1 lavas. Residual magma from the 1977 eruption is thought to have been mixed with magma from the Nāpau Crater region (Garcia *et al.*, 1989). Fissures from episode 1 lay 100-200 m northeast of the episode 59 vents.

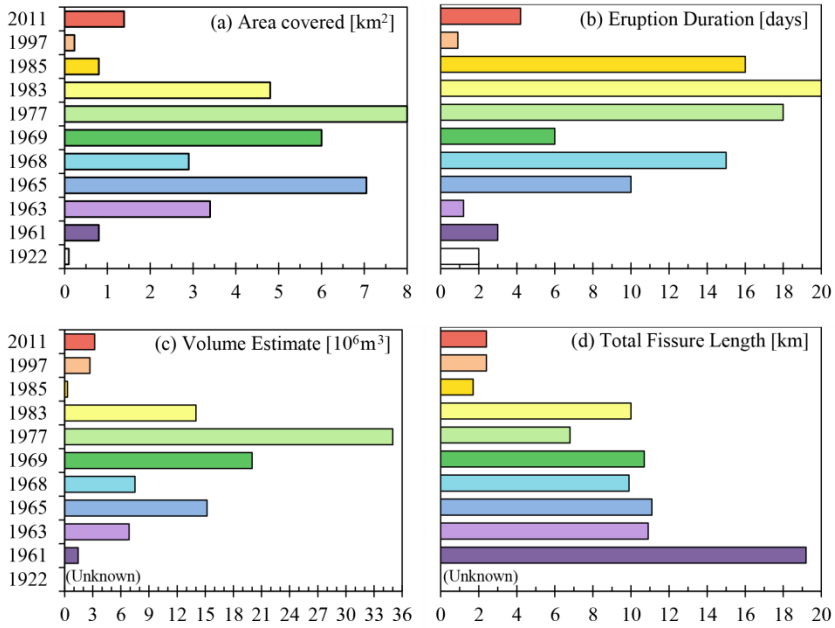

Fig. 3. Summary of key features for historical ERZ eruptions. (a) Area covered by each eruption. (b) Fissure eruption durations. These are based off of the total number of days that the USGS determined the eruptive episode to last; it is not the total amount of hours that lava was ejected. (c) Volume estimates for each fissure eruption. (d) Total eruptive fissure length measured linearly from ends of westernmost to easternmost fissures. Sources: 1922 (Jaggar, 1922); 1961 (Richter *et al.*, 1964; Macdonald *et al.*, 1983); 1963 (Moore & Koyanagi, 1969); 1965 (Wright *et al.*, 1968); 1968 (Jackson *et al.*, 1975); 1969 (Swanson *et al.*, 1976); 1977 (Moore *et al.*, 1980); 1983 (Wolfe *et al.*, 1987); 1985 (Heliker & Mattox, 2003; T. Orr, pers. comm.); 1997 (Thornber *et al.*, 2003; Orr *et al.*, 2015); 2011 (Orr *et al.*, 2015).

Historical Puʻu ʻŌʻō Fissure Eruptions (1983-2011)

1983 (episode 1)

The first episode of the Puʻu ʻŌʻō eruption began in January 1983 and continued intermittently for about three weeks (Fig. 3b; Wolfe *et al.*, 1988). The initial lava outbreak occurred along the

northern edge in Nāpau Crater and progressed 6 km downrift, forming a series of fissures (Wolfe *et al.*, 1988). A magma-storage area is thought to have extended from beneath Nāpau Crater downrift to at least Kalalua Crater (Wolfe *et al.*, 1987; Okamura *et al.*, 1988). The evidence for this storage area includes: (1) the diffusion of the episode 1 seismic swarm as it approached an area just east of Nāpau Crater, (2) the signature of pre-eruptive tumescence, (3) and the deformation at the Kalalua Crater tiltmeter, which was recorded anomalously early (compared to propagation speeds through solid rock) and may have been caused by the propagation of a pressure wave through the reservoir(s) after the intruding episode 1 dike tip intersected it (Okamura *et al.*, 1988). After two subsequent eruptive episodes at vents 3-5 km downrift of Nāpau Crater, eruptive activity focused at a single location, building a pyroclastic cone later named Puʻu ʻŌʻō. A nearly continuous supply of magma from the summit is thought to refill a shallow reservoir under the Puʻu ʻŌʻō cone via a ~3 km deep conduit within the ERZ (e.g., Wolfe *et al.*, 1987, Hoffman *et al.*, 1990).

1985 (episode 35)

Three other Puʻu ʻŌʻō episodes (35, 54, and 59) had eruptive fissure systems in the Nāpau Crater area (Fig. 2). Episode 35 in July 1985 involved a fissure eruption that propagated uprift from Puʻu ʻŌʻō into the area immediately south of and parallel to the episode 59 eastern fissure system (Figs. 2 & 3), ranging from 170-250 m away (T. Orr, pers. comm.). This event was likely shallowly fed (0.5 km) from Puʻu ʻŌʻō (Heliker *et al.*, 2003). Based on the steep geothermal gradient above depths of 1.6 km within the ERZ (Mittelstaedt & Garcia, 2007), residual magma from episode 35 was shallow enough to be fully crystallized before episode 59.

1997 (episode 54)

The brief (~23 hours long) episode 54 eruption in January 1997 followed the collapse of the Puʻu ʻŌʻō cone (Harris *et al.*, 1997). It is thought that passive rift opening (deep rift dilation and slip on Kīlauea's south flank décollement decreased minimum horizontal stresses in the upper few kilometers of the rift zone) caused fracturing that reduced the magmatic overpressure in the main rift conduit (Owen *et al.*, 2000). The passively emplaced dike diverted magma that was once on its way to Puʻu ʻŌʻō and also drew magma uprift from Puʻu ʻŌʻō towards Nāpau Crater (Owen *et al.*, 2000). Episode 54 magma is hypothesized to be from Puʻu ʻŌʻō's shallow reservoir and, prior to eruption, had interacted with stored magma under the Nāpau Crater area (Garcia *et al.*, 2000).

2011 (episode 59)

Episode 59 (the 'Kamoamoa' eruption) started March 5, 2011, and continued for 4.2 days. It followed months of inflation at Kīlauea's summit, rising lava lake levels at the summit and Pu'u 'Ō'ō, and an increase in upper ERZ seismicity (Orr *et al.*, 2015). Episode 59 is thought to have resulted from an over-pressurization of the magma plumbing system between the summit reservoir and Pu'u 'Ō'ō (Lundgren *et al.*, 2013). A 2.4-km-long fissure system developed just east of Nāpau Crater along two main fissures, designated 'east' and 'west' by Orr *et al.* (2015). These fissures formed 100-250 m south of and parallel to those from episodes 1 and 54 in the area east of Nāpau Crater (Fig. 2). Detailed field observations for the episode 59 eruption are given in Appendix A of Orr *et al.* (2015).

The day prior to the onset of episode 59, eight low-magnitude (<2.5) earthquakes (2-4 km depth) occurred between the summit and Hi'iaka Crater (Fig. 1; episode 59 earthquake data are from B. Shiro, unpublished data). On March 5th, the day of the first lava outbreak, <20 low-magnitude earthquakes occurred uprift of Pauahi Crater (Fig. 1) and in the summit region. An earthquake swarm downrift localized at a depth of ~3 km in the general area between Makaopuhi and Nāpau Craters. This was accompanied by rapid deflation at Pu'u 'Ō'ō and the summit, and was followed shortly afterward by the collapse of Pu'u 'Ō'ō's crater floor and the draining of the summit lava lake (lake level dropped ~143 m; Orr *et al.*, 2015). On March 6th, earthquakes were recorded at the summit and near Nāpau Crater, but none were recorded in the area spanning from the upper ERZ downrift to just east of Nāpau Crater. During the remainder of episode 59 (from March 7-9), only 10 earthquakes (all <3.0 magnitude, <3 km depth) were recorded. These 10 earthquakes occurred in the summit region; the upper to middle ERZ remained aseismic. Episode 59 fissures erupted sporadically until the morning of March 8th, when activity became localized on the easternmost and westernmost vents (E-5 and W-1, respectively; Fig. 4). After activity on vent E-5 ceased, lava issued only from vent W-1 until the eruption ended on March 9th (Fig. 4).

A pocket of cooler, rift-zone-stored magma is thought to have mixed with incoming more MgO-rich dike magma during episode 59 (Thornber *et al.*, 2015). This model was refined to suggest incoming magmas were intruded from both uprift and downrift of the fissure system (Orr *et al.*, 2015). The shape, location, and behavior of the dike was interpreted using interferometric synthetic aperture radar (InSAR) and continuous GPS data sets (Lundgren *et al.*, 2013). The uprift portion of the dike is thought to have risen from a depth of 2-3 km whereas the downrift

portion of the dike was interpreted as intruding from a somewhat shallower depth (~2 km; Lundgren *et al.*, 2013). Alternatively, vertical displacement in the InSAR data for the Nāpau Crater area has been interpreted to reflect the inflation of a magma reservoir ~5 km under Nāpau Crater (Baker & Amelung, 2015). The excellent spatial and temporal coverage of samples collected during episode 59 (Orr *et al.*, 2015) provide a comprehensive suite for evaluating the pre-eruptive history and temporal evolution of episode 59 lavas (Fig. 4).

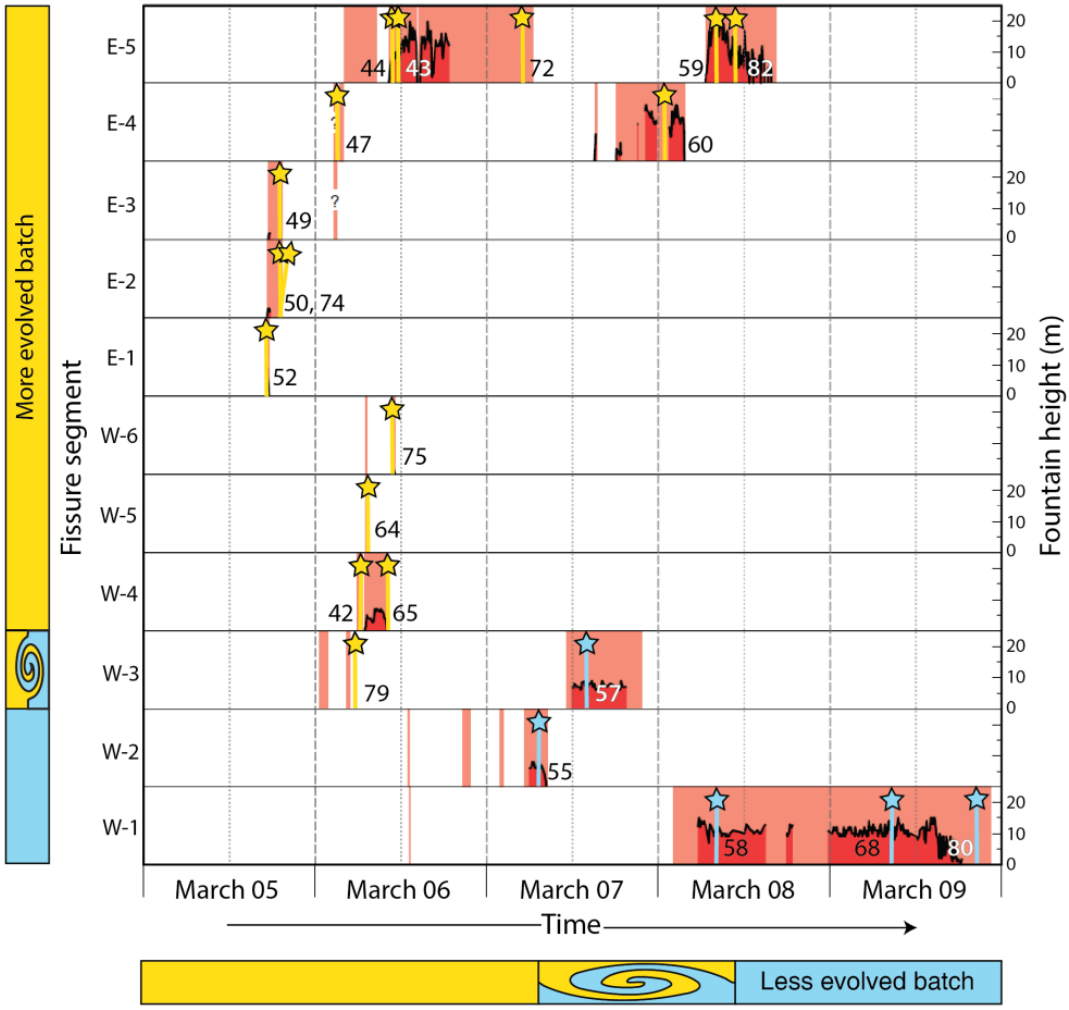

Fig. 4. Temporal variation in effusive activity along each of the 11 eruptive fissures from episode 59. Figure modified from Orr *et al.*, 2015 to show episode 59 sample suite used in this study. Pink/red areas represent periods of fissure activity. Fountain height denoted by black line when quantifiable. Yellow stars represent samples from the geochemically more evolved batch; light-blue stars represent samples from the geochemically less evolved batch. Black or white numbers next to each sample marker represent the last two digits in the episode 59 sample name (i.e. KE59-2944 has been shortened to 44).See Fig. 2 for fissure segment locations (W, western fissures; E, eastern fissures) and Appendix B for sample collection locations.

SAMPLES

The Nāpau Crater area was sampled along ~4 km of the ERZ from 1.2 km W to 2.7 km ENE of Nāpau Crater (as measured from the Nāpau Crater Trail's end; Fig. 2). Spatter and flow samples (30) were collected in or near vents for the 1922, 1963, 1965, 1968, 1983 (episode 1), and 2011 (episode 59) eruptions in May, 2016 (Appendix B). These samples are labeled with the collection region (Kīlauea ERZ), year erupted, and field sample number (e.g., KE1963-01). Twenty-one additional samples from episode 59 (Appendix A) and one from the 1977 eruption were obtained from the USGS. The 21 episode 59 samples are labeled with the collection region (Kīlauea ERZ), Pu'u 'Ō'ō episode number, and Pu'u 'Ō'ō field sample number (e.g., KE59-2942). The 1977 samples are labeled with the collection location (Kīlauea), year erupted, and field sample number (e.g., KI-77-11). Four additional samples from episode 1, five from episode 54, five from episode 58, and four from episode 60 were obtained from a University of Hawai'i at Mānoa collection. The samples from episode 1 and episode 54 were reanalyzed with the other samples to create an internally consistent data set (compositions of these samples from episodes 1 and 54 were originally published in Garcia *et al.* [1989] and [2000], respectively). Episode 1 samples are labeled using the same USGS format as the episode 59 samples; episode 54 samples are labeled by eruptive vent; episode 58 and 60 samples are labeled by date of eruption.

ANALYTICAL METHODS

Olivine and glass compositions were determined using the JEOL Hyperprobe JXA-8500F at the University of Hawai'i at Mānoa. Olivine analyses were conducted using an accelerating voltage of 20 keV, a beam current of 50 nA, and a beam diameter of 1-2 μm (except for three episode 58 olivine crystals for which a beam current of 200 nA was used). Peak counting times were 30 s (Si, Fe, Ni, Mg, Ca), and 15 s for backgrounds on each side of the peak. Standard olivine crystals San Carlos USNM 111312/444 and Springwater USNM 2566 were analyzed periodically to check for instrument drift (Jarosewich *et al.*, 1980). Calibration was based on the San Carlos olivine USNM 111312/444 (Si, Fe, Mg), Cal-Tech Ni-ol GRR-192 (Ni), and Diopside-2 UCLA or Kakanui Augite USNM 122142 (Ca) standards. Drift corrections (1%) were made for SiO_2 and MgO concentrations based on these standards for the three episode 58 olivine profiles. Background fits were linear for all elements. Oxygen was calculated by cation stoichiometry and included in the matrix correction. ZAF matrix corrections were applied based

on the algorithm developed by Armstrong (1988). Analytical precision based on two standard deviations of analyses of the San Carlos and Springwater olivine standards is 0.4 wt. % for Si, 0.3 wt. % for Fe, 0.2 wt. % for Mg, and 0.01 wt. % for Ni and Ca. Olivine core data is based on an average of two spot analyses in each crystal. Olivine profiles consisted of 13 to 52 (average of 25) spots per traverse with 1.1 to 4.2 (average of 2.1) μm spacing.

Glasses were analyzed using an accelerating voltage of 15 keV, a beam current of 10 nA, and a beam diameter of 10 μm. Peak counting times were 50 s (Si, Ti), 60 s (Al, K, P), 70 s (Fe), 40 s (Mn, Ca), 80 s (Mg), and 30 s (Na), with background times half as long on each side of the peak. Sodium was measured first to minimize loss due to volatilization. Basaltic glass standards A99 USNM 113498/1 and VG-2 USNM 111240/52 were run as internal controls to monitor drift (Jarosewich *et al.*, 1980). The A99 standard is a Kīlauean glass with a composition similar to episode 59 lavas. Drift corrections (1%) were made for SiO_2 and Na_2O concentrations based on these standards. Glass calibration was based on the following standards: A99 USNM 113498/1 (Si, Ti, Al, Fe, Mg, Ca), Verma garnet (Mn), Amelia albite (Na), orthoclase (K), and fluorapatite USNM 104021 (P). Background fits were linear for all elements. ZAF matrix corrections were applied based on the algorithm developed by Armstrong (1988). Analytical precision based on two standard deviations of analyses of the A99 and VG-2 glass standards is 0.5 wt. % for Si, <0.2 wt. % for Al, Fe, Mg, Ca, and Na, and <0.1 wt. % for Ti, Mn, K, and P. Data is based on an average of four to six spot analyses in glass, except samples KE1963-04, which is based on three spots, and samples KE 1963-03, KE1983-13, and KE1983-27, which are based on an average of two spots.

Whole-rock XRF analyses were made for major and trace elements (Ba, Rb, Sr, Y, Zr, Nb, Ba, La, Zn, Ni, Cr, and V) at the University of Massachusetts at Amherst (for procedural methods, see Rhodes & Vollinger, 2004). Samples were coarsely crushed (1-8 mm) with a tungsten-carbide coated hydraulic press, ultrasonically cleaned in Millipore water, then dried for 24 hours at 40 °C. Samples were hand-picked to remove fragments with signs of alteration to ensure only the freshest parts of each sample were analyzed. The analytical precision for XRF analyses is based on repeated analyses (n = 21) of the BHVO-1 standard that ran with the upper to middle ERZ sample suite and is <0.1 wt. % for Si and Al, 0.005 wt. % for Ti, 0.02 wt. % for Fe and Na, 0.002 wt. % for Mn, 0.04 wt. % for Mg, 0.06 wt. % for Ca, and 0.03 wt. % for K and P.

RESULTS

Petrography

Modal mineralogy was determined for 26 representative samples from the Nāpau Crater area using 1000 counts per sample (excluding vesicles) for phenocrysts (>0.3 mm wide), microphenocrysts (0.1-0.3 mm wide), and matrix (glass and microlites, <0.1 mm wide). The historical Nāpau Crater area lavas range from aphyric to weakly olivine and/or clinopyroxene phyric (samples have ≤2.0 vol. % total phenocrysts; Table 2). Sample vesicularity ranges widely from 17-74 vol. % with a mean of 44 vol. % (Table 2). Olivine, clinopyroxene, and plagioclase are present in all samples at least as a microlitic phase.

Table 2: Modes of representative samples from fissure eruptions in the Nāpau Crater area.

Sample	Ol ph	Ol mph	Cpx ph	Cpx mph	Pl mph	Matrix	Ves
Pre-Puʻu ʻŌʻō							
KE1922-09	-	-	-	0.8	0.6	98.6	54.2
KE1922-08	-	-	0.8	0.2	-	99.0	29.9
KE1963-14	0.6	-	-	2.4	-	97.0	32.1
KE1965-17	0.3	-	0.1	0.1	-	99.5	47.6
KE1965-19	0.4	0.1	0.5	0.3	0.1	98.6	58.9
KE1968-35	-	-	-	0.6	-	99.4	51.8
KE1968-05	1.1	0.5	0.9	0.8	-	96.7	44.3
Puʻu ʻŌʻō - Episode 1							
KE1-49	-	0.1	-	2.1	2.1	95.7	ukn
KE1-5	-	-	-	0.2	0.6	99.2	ukn
KE1-37	-	-	-	2.5	5.0	92.5	ukn
Puʻu ʻŌʻō - Episode 54							
Vent F	-	*	-	0.1	0.4	99.5	47.9
Vent A	-	0.1	-	0.5	-	99.4	73.5
Vent B	-	0.1	-	0.1	0.2	99.6	52.8
Vent D	-	0.1	-	0.3	0.2	99.4	62.5
Vent E	-	0.2	-	0.6	0.3	98.9	51.7
Puʻu ʻŌʻō - Episode 59							
KE59-2955	-	0.2	-	0.4	0.6	98.8	22.7
KE59-2958	-	*	-	0.9	1.3	97.8	17.0
KE59-2980	*	0.4	-	1.0	0.3	98.3	32.4
KE59-2979	-	*	-	0.2	0.2	99.6	52.3
KE59-2942	-	*	-	0.1	0.7	99.2	35.5
KE59-2964	-	*	-	0.5	0.9	98.6	37.9
KE59-2975	-	*	*	0.8	0.6	98.6	27.9
KE59-2952	-	*	-	0.3	0.5	99.2	54.4
KE59-2974	-	-	-	0.4	1.0	98.6	43.5
KE59-2949	-	-	-	0.3	0.3	99.4	27.1
KE59-2947	-	-	-	0.4	0.6	99.0	55.3
KE59-2943	-	-	-	0.6	0.7	98.7	42.0
KE59-2982	-	0.6	-	0.5	0.7	98.2	33.0
KE59-2972	-	-	-	0.6	0.6	98.8	40.3

Notes: All values are given in volume percent, based on 1000 counts/ sample (excluding vesicles) for phenocrysts (> 0.3 mm), microphenocrysts (0.1-0.3 mm), and matrix (glass and microlites, < 0.1 mm wide). *Denotes samples where one crystal was observed but not counted. The 1σ uncertainty is ~0.2 vol. % based on Folk (1968).Vesicularity = vesicle counts/ (vesicle counts + 1000). Ol, olivine; Cpx, clinopyroxene; Pl, plagioclase; ph, phenocrysts; mph, microphenocrysts; Ves, vesicularity; ukn, unknown. Data for episode 1 samples (KE1-49, -5, -37) are from Garcia *et al.* (1989). Collection locations are provided in Appendix B.

1963, 1965, and 1968 samples

Olivine and/or clinopyroxene phenocrysts are small (≤1.1 mm in diameter) and are present in four of the five examined samples from the 1963-1968 fissure eruptions (Table 2). Some olivine phenocrysts appear in clusters with anhedral to subhedral clinopyroxene, whereas others are isolated and euhedral. Spinel inclusions are common within olivine phenocrysts and microphenocrysts. Isolated clinopyroxene phenocrysts and microphenocrysts are subhedral to euhedral. Some clinopyroxene microphenocrysts display sector zoning, a disequilibrium texture consistent with rapid crystal growth (e.g., Wass, 1973; Welsch *et al.,* 2016).

Pu‘u ‘Ō‘ō samples

Petrographic information for episode 1 lavas is from Garcia *et al.* (1989). Episode 1 lavas contain rare (<0.1 vol. %) phenocrysts (0.5-1 mm) of plagioclase, augite, and olivine. Microphenocrysts (0.1-0.5 mm) of these phases are mostly euhedral and range widely in total abundance (0.3-9.2 vol. %). Resorbed grains of all phases are present, but rare. Episode 54 lavas range from aphyric to very weakly olivine and or plagioclase phyric (samples have ≤0.3 vol. % total phenocrysts [0.5-1 mm]; Garcia *et al.,* 2000). Olivine phenocrysts show normal zoning and some are resorbed (Thornber *et al.,* 2003). Clinopyroxene phenocrysts are rounded or euhedral and have normal and/or reverse zoning (Thornber *et al.,* 2003). Lavas from vent F are distinguished from other vents by their higher plagioclase microphenocryst content (1.6 wt. % in Vent F lava as compared to an average of 0.5 from vents B and D lavas; Garcia *et al.,* 2000). Furthermore, the only orthopyroxene crystal reported in episode 54 lavas was found in a vent F sample; the crystal is resorbed and has reverse zoning (Thornber *et al.*, 2003).

Almost all of the episode 59 lavas lack phenocrysts (Table 2). Only one olivine (0.32 mm wide) and one clinopyroxene phenocryst (0.36 mm wide) was found in the thin sections of episode 59 lavas (Table 2). Episode 59 lavas were previously reported to contain phenocrysts of olivine, clinopyroxene, and plagioclase that show an array of disequilibrium textures indicative

of a complex heating and cooling history (Orr *et al.*, 2015). Thornber *et al.* (2015) reports that many episode 59 olivine microphenocrysts show reverse or complex zoning.

Olivine microphenocrysts and microlites are almost always clustered with plagioclase with or without clinopyroxene. Rarely, olivine occurs as an isolated crystal. Clinopyroxene microphenocrysts are commonly subhedral to euhedral and cluster with plagioclase. Faint sector zoning in one or more clinopyroxene microphenocrysts was observed in nearly half of the episode 59 thin sections. Plagioclase microphenocrysts are either isolated, in crystal clots with euhedral plagioclase microlites, or clustered with clinopyroxene. Rarely, plagioclase microphenocrysts have a sieve texture. Oscillatory zoning in one or more plagioclase microphenocrysts was observed in nearly half of the episode 59 thin sections, but these samples do not necessarily correspond to the samples with sector zoning in clinopyroxene, (although there is some overlap).

No temporal or spatial trends were observed in the mineral abundances and textures of episode 59 lavas (Table 2; Fig. 4). The lavas erupted from the Eastern fissure system are petrographically indistinguishable from those erupted from the Western fissure system (Table 2; Fig. 4). Likewise, mineral modes and textures from early lavas parallel those from late in the eruption (Table 2; Fig. 4).

Olivine chemistry

Microprobe analyses were made of olivine from the 1965, 1968, 1997 (episode 54), and 2011 (episode 59) eruptions to determine their compositions and zoning patterns (Appendix C). These data are essential for assessing the role of magma mixing in creating the composition of the episode 59 lavas and for the timescales of magma mixing. Microphenocrysts, microlites, and one phenocryst were analyzed in episode 59 lavas (n = 47), whereas phenocrysts and microphenocrysts were analyzed from episode 54 (n = 6), 1965 (n = 4), and 1968 (n = 7) lavas. Olivine cores from the more evolved episode 59 lavas span from ~Fo_{74-78}. Crystals from the less evolved batch are bimodal with a broader distribution (Fo_{74-82}) that encompasses the range of the more evolved batch (Fig. 5). Cores from episode 54 range from Fo_{82-83}, and those from 1965 and 1968 range from Fo_{77-86} (Fig. 6).

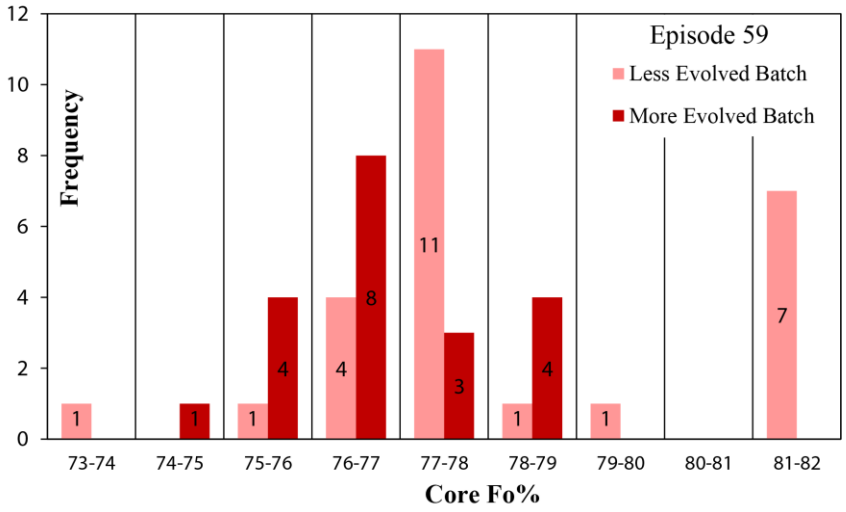

Fig. 5. Forsterite (Fo%) in episode 59 olivine cores. Olivine core data in Appendix C. Number on each bar represents the frequency of core data in each bin. Fo calculated as [Mg/(Mg+Fe)]*100%. The 2σ for Fo% is 0.10%. Cores from the more evolved batch span from ~Fo_{74-78}. Crystals from the less evolved batch have a broader distribution (Fo_{74-82}) that encompasses the range of the more evolved batch and are bimodal.

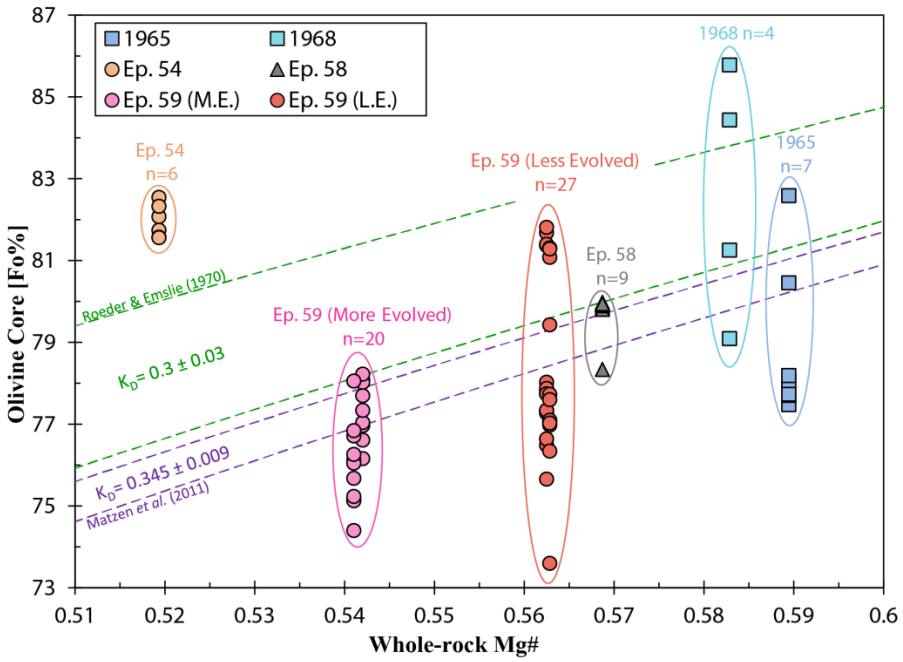

Fig. 6. Middle ERZ olivine cores (Fo% vs. whole-rock Mg#). Mg# assumes Fe^{2+} = 0.9*total Fe based on iron redox determinations of Hawaiian tholeiites (Moore & Ault, 1965). Dashed olivine-melt disequilibrium lines are from Matzen *et al.* (2011; purple) and Roeder & Emslie (1970; green). The ranges between each pair of equilibrium lines are interpreted to represent olivine compositions that are in Fe-Mg equilibrium with their host melt (Roeder & Emslie, 1970; Matzen *et al.*, 2011). Episode 58 data (erupted from Pu‘u ‘Ō‘ō vent) are from Lynn *et al.* (2017). The 2σ error bars are within the size of the symbol.

Backscattered electron (BSE) images of olivine from episode 54 and 59 lavas show either normal or complex zoning patterns (Fig. 7). The complex zoning patterns include both normal and reverse zoning within single crystals (Fig. 7) and are present in 18 out of 25 profiles analyzed (2/5 from episode 54 and 16/20 from episode 59; Fig. 8). In each of the 18 complexly zoned olivine crystals, there is a more Mg-rich region that exhibits normal zoning to the rim (Fig. 7). This thin (~6-48 μm) more Mg-rich region that encircles the core represents a spike in Fo (forsterite; calculated as [Mg/(Mg+Fe)]*100%) content (Fig. 7).

Rim-to-core profiles were analyzed on 20 crystals from episode 59 and five from episode 54 to quantify the change in Fo concentration observed in BSE imagery (Fig. 8). The cores of the 18 complexly zoned olivine crystals show normal or reverse zoning from the core to the base of the more Mg-rich peak (Fig. 7). One half of the crystals exhibit normal zoning from the core to the base of the more Mg-rich peak, whereas the other half show reverse zoning from the core to the base of the more Mg-rich peak (1/2 olivine crystals from episode 54 and 8/16 crystals from episode 59 are either normally or reversely zoned from the core to the more Mg-rich peak.) The Fo range in episode 59 olivine crystals is 0.3-2.5% Fo, with an average of 1.0% Fo. Rim compositions from episode 54 olivine crystals tightly converge to Fo_{79-80}, and those from episode 58 tightly converge to $Fo_{78-79.}$ Episode 59 olivine crystals, however, have a much wider range in rim composition (Fo_{71-79}; Fig. 8).

Most of the 47 episode 59 olivine cores analyzed (75%) are out of Fe-Mg equilibrium with their host melt (15/20 for the more evolved batch, 20/27 for the less evolved batch; Fig. 6). Melt compositions for episode 59 reflect the whole-rock compositions due to the virtual absence of phenocrysts and the low abundance of microphenocrysts (0.4-2.2%, average of 1.2%; Table 2) in these samples. The crystals from 1965 and 1968 lavas with core compositions that plot below the olivine-liquid equilibrium field (Fig. 6) exhibit reverse zoning (2.0-3.5% Fo). The crystals from 1965 and 1968 lavas that plot in or above the equilibrium fields display normal zoning or are unzoned. Olivine cores from episode 54 are all too forsteritic to be in equilibrium with the evolved composition of their host rock (Fig. 6). Thus, they must have grown in a more magnesian melt. Olivine cores with >81% Fo from the less evolved batch of episode 59 lavas are similar to the episode 54 cores in Fo content (Fig. 6, Fig. 8). The rest of the olivine cores from the less evolved batch of episode 59 lava (those with <81% Fo) mostly plot below the equilibrium fields, and may have been derived from a more Fe-rich melt. The more evolved

batch of episode 59 olivine has core contents that are similar to the group of olivine with <78% Fo from the less evolved batch (Fig. 6). Crystal accumulation could cause the majority of olivine cores to plot below a line of equilibrium (Garcia *et al.*, 2000), however, this is an unlikely magmatic process to associate with episode 59 due to the lack of phenocrysts and the sparseness of microphenocrysts in episode 59 lavas (Table 2).

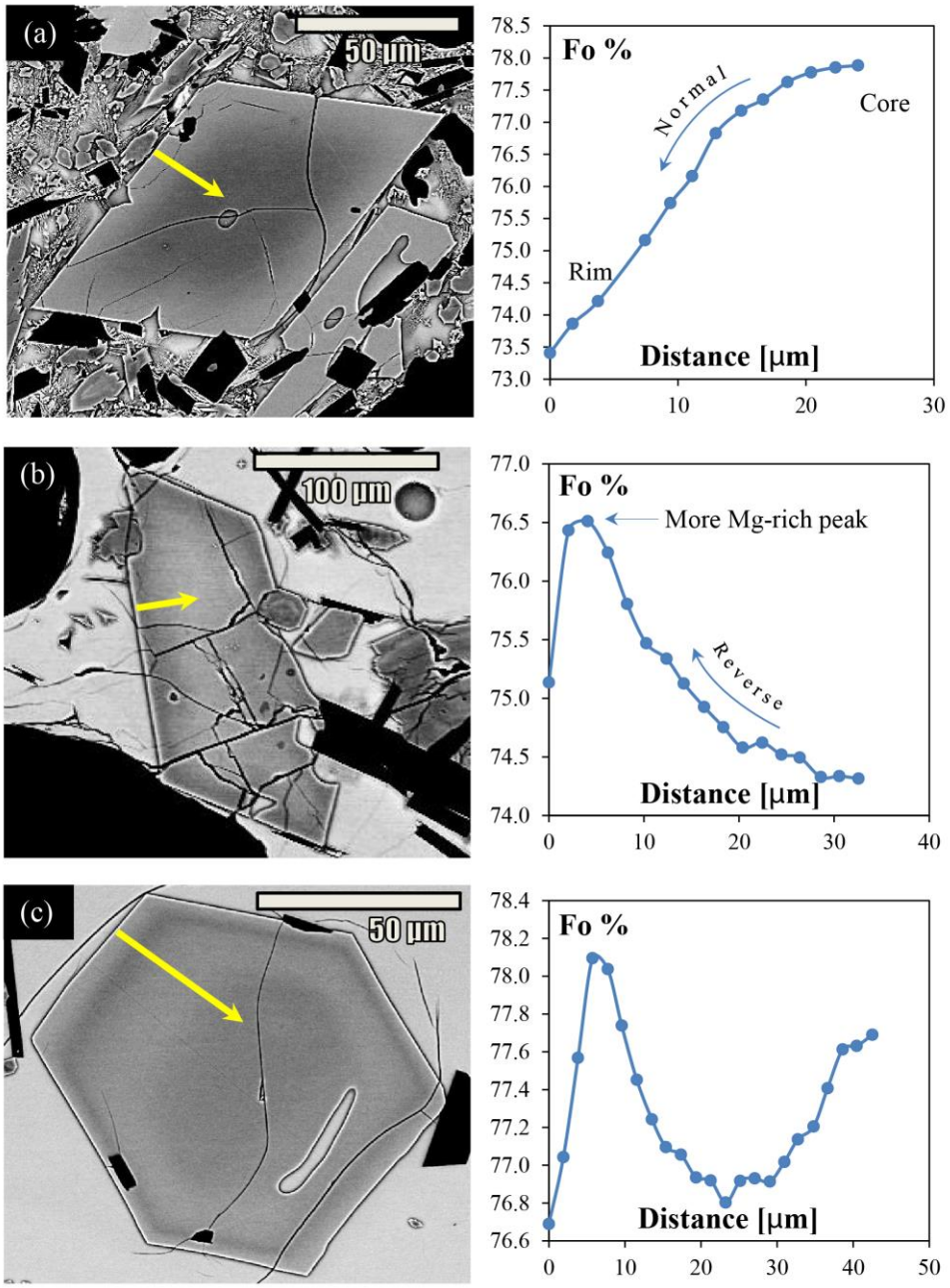

Fig. 7. BSE images and Fo% profiles of episode 59 olivine microlites (<0.1 mm). BSE images collected at 20 keV accelerating voltage. Yellow arrows mark the traversed path shown by the

blue profile analysis to the right of each olivine image. Profiles plot Fo% vs. rim-to-core distance (μm) in olivine from episode 59 to highlight examples of normal and/or complex zoning. The 2σ for Fo% is 0.10%. (a) Normal zoning in olivine (Fo concentration decreases from core to rim). (b) Complex zoning in olivine (Fo concentration increases from core to more Mg-rich peak [reverse zoning] and then decreases to rim [normal zoning]). (c) Complex zoning (Fo concentration decreases from core to base of Mg-rich peak at 23 μm [normal zoning], increases to peak near 6 μm [reverse zoning], then decreases to rim [normal zoning].

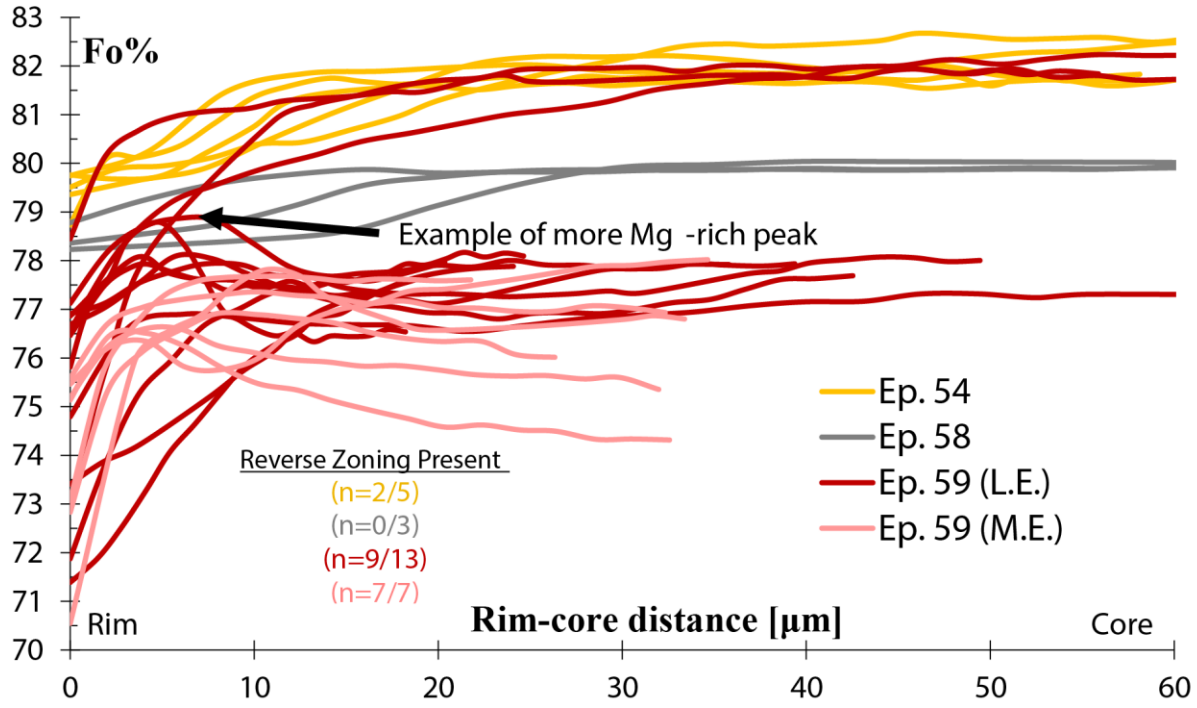

Fig. 8. Fo% vs. rim-to-core distance (μm) in episodes 54, 58, and 59 olivine. The 2σ for Fo% is 0.10%.

Glass geochemistry

Glass from 54 Nāpau Crater area samples that erupted from 1963 to 2011 were analyzed by microprobe for major and minor elements (Appendix D). The glasses have a wide range of MgO and K_2O contents (5.3-7.2 wt. % MgO; 0.51-0.76 wt. % K_2O; Fig. 9a). The glasses from 1963 and 1965 lavas have MgO contents >6.4 wt. %, whereas glasses from episodes 1, 54, and 59 lavas have <6.4 wt. % (Fig. 9a). The 1968 glasses have intermediate MgO values ranging from 6.1 to 6.7 wt. % (Fig. 9a, Appendix D).

MgO variation diagrams for the Nāpau glasses show a kink at 6.6-6.7 wt. % MgO for CaO and Al_2O_3 (Fig. 9b & 9c). The sharp decrease at ~6.7 wt. % MgO in CaO marks the onset of clinopyroxene crystallization. This is consistent with the observation of clinopyroxene as a

microphenocryst in the samples. The kink near 6.6-6.7 wt. % MgO on the Al_2O_3 vs. MgO plot is indicative of the beginning of plagioclase fractionation, which is also consistent with petrographic observations (Table 2). The order of crystallization in this suite (olivine followed by clinopyroxene then plagioclase) matches the order observed by Wright & Okamura (1977) for Makaopuhi lava lake samples.

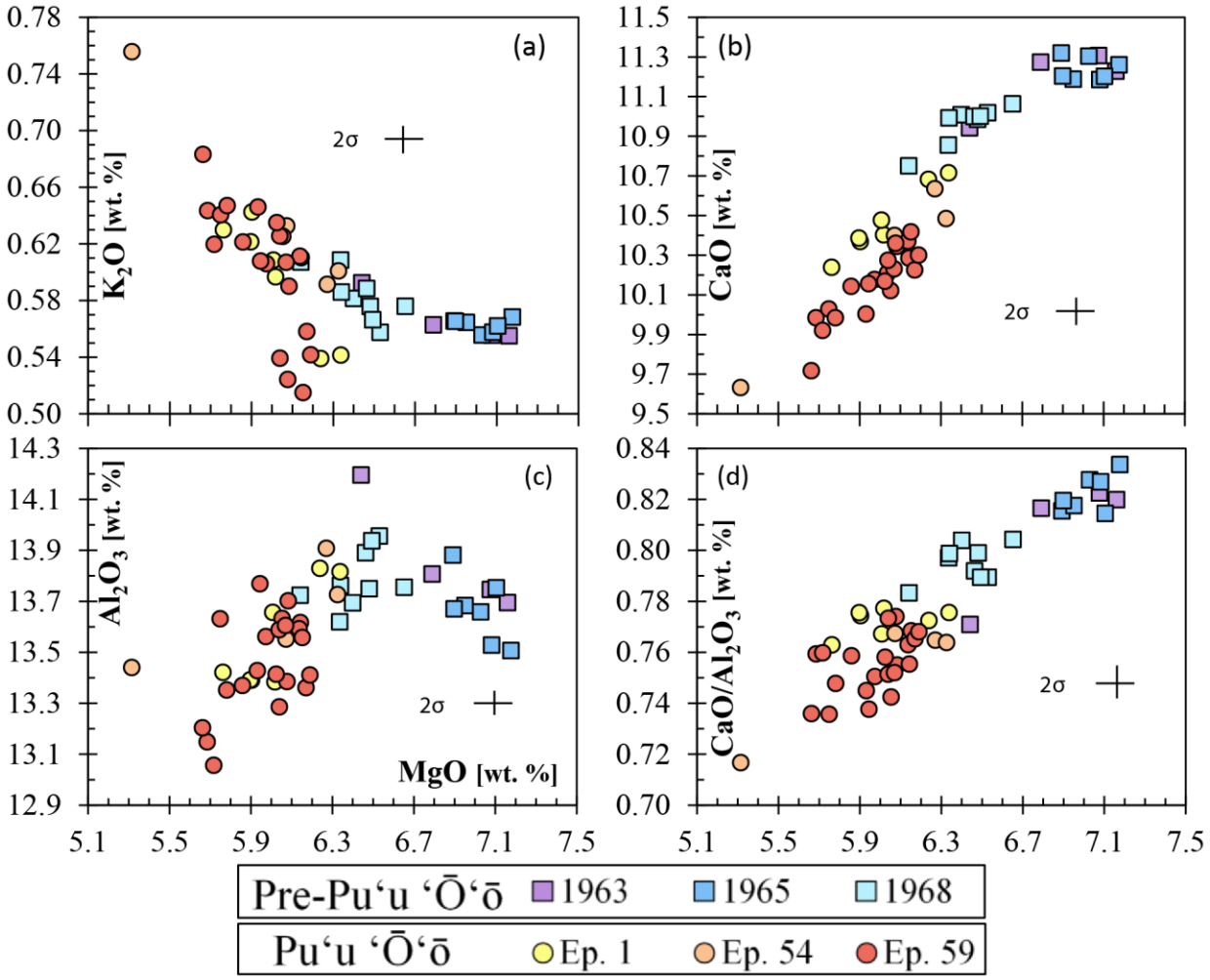

Fig. 9. Glass compositions (in wt. %) from Nāpau Crater area lavas. Data in Appendix D. (a) K_2O vs. MgO variation. (b) CaO vs. MgO variation. (c) Al_2O_3 vs. MgO variation (d) CaO/Al_2O_3 variation.

Two geothermometers were developed for Kīlauea ERZ glass compositions (Helz & Thornber, 1987). The MgO-based thermometer is applicable to glasses with only olivine fractionation, as indicated by a horizontal trend on a CaO/Al_2O_3 vs. MgO plot. The CaO-based thermometer is relevant for glasses that coexist with olivine, clinopyroxene, and plagioclase. The

CaO-based glass thermometer is employed for this suite of Nāpau samples because they all contain olivine, clinopyroxene, and plagioclase (at least as microlitic phases; Table 2). This is consistent with the broad linear correlation (r^2= 0.86) for CaO/Al_2O_3 vs. MgO found for all lavas, which form a positive slope that is indicative of crystallization beyond olivine-only (Fig. 9d).

Results from geothermometry calculations yield an overall range in eruption temperatures from 1128-1156 °C (Appendix D; uncertainty in inferred quenching temperatures is ± 8-10°C; Helz & Thornber, 1987). Samples from 1963, 1965, and 1968 have higher temperatures (1147-1156 °C) whereas samples from episodes 1, 54, and 59 have somewhat lower temperatures (1128-1146 °C). Thermometry calculations for episode 59 glasses yielded a temperature range of 1129-1141 °C. Temperatures for the more evolved and less evolved batches of episode 59 lavas are indistinguishable from each other within error. These temperatures are consistent with MgO-based values (1130-1145 °C) for episode 59 from Orr *et al.* (2015).

Whole-rock geochemistry

Eighty upper to middle ERZ samples were analyzed by XRF for major and trace elements (Table 3). This suite of tholeiitic basalts varies in MgO content from 5.4-9.4 wt. %, with the lavas from 1963 and 1965 containing higher concentrations of MgO (7.2-7.6 wt. %) than the Pu‘u ‘Ō‘ō lavas (5.7-7.1 wt. %), excluding episode 35 (Table 3). Samples from 1968 have an intermediate MgO range (6.6 and 7.1 wt. %) except for one higher-MgO sample (KE1968-06) with 8.2 wt. % (Fig. 10). Lavas from episode 59 are subdivided into two geochemically distinct magma batches: one more evolved (6.1-6.3 wt. % MgO) and one slightly less evolved (6.5-6.6 wt. % MgO) end-member (Fig. 10a). The less evolved batch of episode 59 lavas (erupted from the three westernmost vents during March 7-9) has lower amounts of K_2O (0.46-0.48 wt. %) than the more evolved batch (0.56-0.60 wt. %; Fig. 11). Samples that erupted from the eastern vents have more evolved compositions (Fig. 11a). The western vents (W-3, -4, -5, and -6) also erupted samples that were more evolved for ~5 hours on the morning of March 6th (Fig. 11a). Vent W-3 issued samples from both the more and less evolved batches (Fig. 11c), whereas vents W-1 and W-2 erupted samples from only the less evolved batch (Fig. 11d).

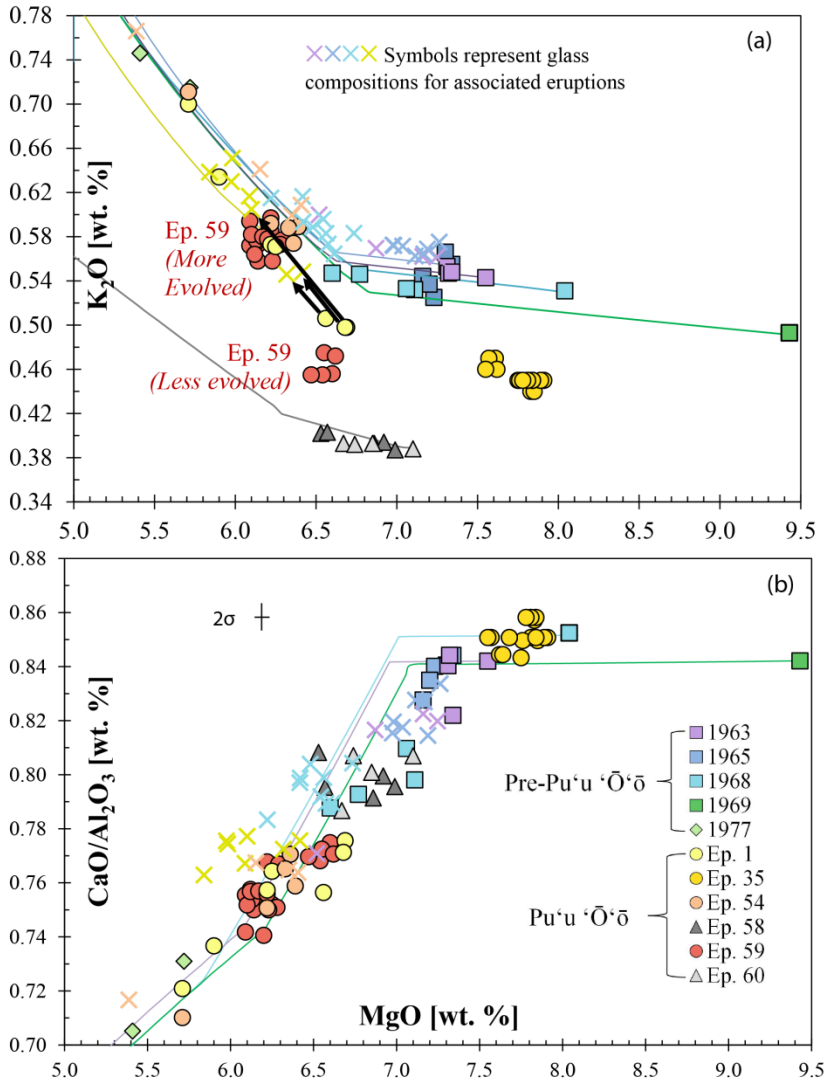

Fig. 10. Whole-rock MgO variation diagrams for K_2O and CaO/Al_2O_3 from upper to middle ERZ lavas. Data for samples DAS69-3-2 and KI-77-11 are from Pietruszka *et al.* (in preparation); episode 35 samples are from Thornber *et al.* (2002); episodes 58 and 60 samples are from Garcia (unpublished data). Glass compositions are plotted as '×' symbols for 1963, 1965, 1968, and episode 1 lavas and represent a more fractionated composition of each associated lava sample. More glass data than whole-rock data is available for each sample suite and not all whole-rock compositions have a corresponding glass composition. Crystal fractionation trends (plotted as solid or dashed colored lines) were calculated for select samples using Petrolog (Danyushevsky & Plechov, 2011) and represent potential compositions of fractionated magmas from 1963, 1965, 1968, 1969, and episode 1. Input parameter values are representative of Kīlauean magmatic conditions. Sources for input parameters: pressure (Garcia *et al.*,1989) ; oxygen fugacity (Rhodes & Vollinger, 2005); H_2O content (Clauge *et al.*, 1995). (a) K_2O vs. MgO variation. The 2σ error bars are within the size of the symbol. Legend shown in Fig. 10b. Three examples of episode 1 lavas' liquid line of descent are expressed by the black arrows, which connect their whole-rock and glass compositions. Petrolog models ran at 1 kbar, at QFM, and with 0.4 wt. % H_2O. (b) CaO/Al_2O_3 vs. MgO variation. Petrolog models ran at 1.5 kbar, -0.5 QFM, and with 0.5 H_2O.

Table 3: XRF analyses of whole-rock major oxide concentrations (in wt. %) for upper to middle ERZ samples.

Sample	SiO_2	TiO_2	Al_2O_3	$Fe_2O_3^*$	MnO	MgO	CaO	Na_2O	K_2O	P_2O_5	Total
Pre-Puʻu ʻŌʻō											
KE1922-09	50.55	3.638	13.03	13.68	0.18	5.39	9.21	2.81	0.722	0.412	99.62
KE1922-08	49.99	2.754	13.80	12.56	0.17	6.68	10.79	2.07	0.541	0.291	99.65
KE1963-14	50.16	2.706	13.37	12.16	0.17	7.34	10.99	2.24	0.548	0.288	99.97
KE1963-04	50.06	2.663	13.04	12.33	0.18	7.55	10.98	2.23	0.543	0.286	99.86
KE1963-03	50.04	2.685	13.09	12.27	0.17	7.31	11.00	2.11	0.553	0.289	99.52
KE1963-02	50.21	2.694	13.03	12.30	0.18	7.32	11.00	2.23	0.547	0.288	99.80
KE1965-20	50.00	2.700	13.23	12.25	0.17	7.16	10.95	2.28	0.544	0.287	99.57
KE1965-34	50.21	2.684	13.32	12.29	0.17	7.40	11.06	1.61	0.545	0.286	99.58
KE1965-15	50.00	2.670	13.11	12.27	0.17	7.30	11.02	2.24	0.566	0.285	99.63
KE1965-17	49.92	2.678	13.09	12.29	0.17	7.34	11.05	2.33	0.555	0.283	99.71
KE1965-19	50.18	2.741	13.04	12.44	0.18	7.30	11.06	1.79	0.548	0.287	99.57
KE1968-35	50.10	2.715	13.75	12.41	0.17	6.77	10.90	2.15	0.546	0.287	99.80
KE1968-36	50.13	2.719	13.61	12.49	0.18	7.06	11.02	2.32	0.533	0.283	100.35
KE1968-05	50.00	2.708	13.62	12.45	0.17	7.11	10.87	2.21	0.532	0.284	99.95
KE1968-06	49.95	2.637	12.94	12.60	0.18	8.15	10.80	2.00	0.521	0.277	100.06
KE1968-31	50.13	2.774	13.66	12.49	0.18	6.60	10.76	2.30	0.547	0.300	99.74
DAS69-3-2	49.55	2.456	12.54	12.32	0.19	9.43	10.56	2.05	0.493	0.250	99.85
KI-77-13	50.78	3.213	13.53	12.94	0.18	5.72	9.89	2.66	0.715	0.377	100.01
KI-77-11	50.82	3.438	13.43	13.22	0.20	5.41	9.47	2.69	0.746	0.397	99.82
Puʻu ʻŌʻō - Episode 1											
KE1983-13*	50.08	2.624	13.75	12.27	0.17	6.63	10.79	2.94	0.491	0.271	100.02
KE1983-12*	50.37	2.662	13.99	12.34	0.17	6.68	10.79	2.23	0.498	0.272	100.00
KE1983-11*	50.27	2.651	13.86	12.34	0.17	6.69	10.75	2.52	0.498	0.274	100.02
KE1-53+	50.37	2.914	13.68	12.62	0.18	6.22	10.36	2.39	0.573	0.307	99.74
KE1-58+	50.37	2.884	13.66	12.64	0.18	6.25	10.44	2.41	0.571	0.306	99.71
KE1-38^	50.42	3.299	13.47	13.28	0.18	5.71	9.71	2.61	0.700	0.377	99.76
KE1-25^	50.70	3.176	13.52	13.01	0.19	5.90	9.96	2.59	0.634	0.359	100.04
Puʻu ʻŌʻō - Episode 35											
KE35-404	50.4	2.51	13.3	12.5	0.17	7.76	11.3	2.06	0.45	0.26	99.46
KE35-396	50.4	2.53	13.3	12.5	0.17	7.83	11.4	2.15	0.44	0.26	99.73
KE35-410	50.5	2.53	13.4	12.5	0.17	7.84	11.4	2.09	0.45	0.26	99.89
KE35-425	50.6	2.54	13.4	12.5	0.17	7.55	11.4	2.13	0.46	0.25	99.75
KE35-399	50.5	2.51	13.4	12.5	0.17	7.81	11.4	2.14	0.45	0.26	99.89
KE35-413	50.7	2.54	13.4	12.6	0.17	7.81	11.5	2.18	0.45	0.27	100.36
KE35-414	50.5	2.53	13.4	12.5	0.17	7.78	11.5	2.22	0.45	0.26	100.06
KE35-397	50.4	2.51	13.3	12.5	0.17	7.85	11.3	2.07	0.44	0.26	99.55
KE35-421	50.5	2.54	13.5	12.5	0.17	7.62	11.4	2.14	0.46	0.25	99.83
KE35-408	50.8	2.54	13.4	12.5	0.17	7.89	11.4	2.16	0.45	0.26	100.32
KE35-438	50.7	2.55	13.4	12.5	0.17	7.68	11.4	2.15	0.46	0.25	100.01
KE35-439	50.6	2.54	13.5	12.5	0.17	7.64	11.4	2.16	0.46	0.25	99.97
KE35-412	50.6	2.55	13.4	12.6	0.17	7.84	11.5	2.11	0.45	0.26	100.22
KE35-419	50.5	2.54	13.4	12.5	0.17	7.57	11.4	2.24	0.47	0.25	99.79
KE35-441	50.7	2.55	13.4	12.5	0.17	7.68	11.4	2.19	0.47	0.25	100.06
KE35-389	50.5	2.53	13.4	12.5	0.17	7.91	11.4	2.14	0.45	0.26	100.01
KE35-390	50.4	2.51	13.4	12.5	0.17	7.75	11.3	2.08	0.45	0.25	99.56

KE35-394	50.5	2.52	13.4	12.6	0.17	7.82	11.4	2.1	0.45	0.26	99.96
Pu‘u ‘Ō‘ō - Episode 54											
Vent F	50.44	3.409	13.49	13.15	0.18	5.71	9.58	2.60	0.711	0.381	99.65
Vent A	50.08	2.920	13.56	12.78	0.18	6.39	10.29	2.38	0.589	0.312	99.48
Vent B	50.42	2.973	13.76	12.80	0.18	6.22	10.33	2.35	0.592	0.315	99.94
Vent D	50.64	2.924	13.60	12.74	0.18	6.36	10.48	2.37	0.574	0.308	100.18
Vent E	50.28	2.931	13.50	12.77	0.18	6.33	10.33	2.58	0.588	0.312	99.80
Pu‘u ‘Ō‘ō - Episode 58											
29-Sep-10	50.94	2.397	13.61	12.16	0.19	6.53	11.00	2.18	0.402	0.236	99.65
6-Oct-10	50.92	2.356	13.71	12.12	0.18	6.86	10.85	2.20	0.393	0.222	99.81
20-Nov-10	51.04	2.357	13.62	12.18	0.18	6.92	10.89	2.21	0.394	0.224	100.02
12-Jan-11	51.03	2.397	13.68	12.19	0.18	6.57	10.88	2.21	0.403	0.226	99.77
13-Feb-11	50.85	2.327	13.65	12.11	0.18	6.99	10.86	2.18	0.387	0.221	99.76
Pu‘u ‘Ō‘ō - Episode 59											
KE59-2955	50.40	2.584	13.68	12.56	0.18	6.60	10.60	2.70	0.456	0.256	100.02
KE59-2958	50.55	2.622	13.58	12.56	0.18	6.55	10.49	2.23	0.475	0.267	99.50
KE59-2968	50.76	2.638	13.72	12.44	0.19	6.47	10.56	2.27	0.455	0.261	99.76
KE59-2980	50.65	2.613	13.69	12.58	0.18	6.62	10.55	2.11	0.472	0.267	99.73
KE59-2979	50.52	2.910	13.77	12.83	0.18	6.28	10.34	2.53	0.573	0.308	100.24
KE59-2942	50.51	2.912	13.52	12.76	0.18	6.22	10.38	2.49	0.585	0.305	99.86
KE59-2965	50.58	2.903	13.65	12.65	0.18	6.12	10.33	2.41	0.564	0.300	99.69
KE2011-33	50.40	2.883	13.72	12.83	0.18	6.23	10.29	2.68	0.558	0.304	100.08
KE59-2957	50.72	2.591	13.76	12.41	0.18	6.54	10.57	2.18	0.455	0.255	99.66
KE59-2964	50.43	2.900	13.67	12.80	0.18	6.25	10.28	2.47	0.572	0.310	99.86
KE59-2975	50.25	2.886	13.66	12.90	0.18	6.24	10.26	2.42	0.571	0.309	99.68
KE59-2952	50.45	2.942	13.56	12.90	0.18	6.29	10.40	2.56	0.577	0.313	100.17
KE59-2950	50.57	2.952	13.62	12.70	0.19	6.09	10.29	2.40	0.572	0.305	99.69
KE59-2974	50.37	2.918	13.80	12.80	0.17	6.20	10.22	2.44	0.578	0.311	99.81
KE59-2949	50.52	2.920	13.53	12.86	0.18	6.12	10.25	2.31	0.573	0.312	99.58
KE59-2947	50.52	2.960	13.71	12.84	0.18	6.09	10.17	2.39	0.594	0.325	99.78
KE59-2944	50.68	2.950	13.72	12.70	0.18	6.14	10.29	2.48	0.558	0.306	100.00
KE59-2960	50.72	2.932	13.66	12.67	0.19	6.10	10.27	2.45	0.582	0.311	99.89
KE59-2943	50.23	2.920	13.59	12.81	0.18	6.14	10.24	2.41	0.573	0.311	99.40
KE59-2959	50.71	2.930	13.65	12.68	0.19	6.13	10.29	2.44	0.577	0.309	99.91
KE59-2982	50.84	2.929	13.60	12.91	0.18	6.22	10.28	2.51	0.597	0.315	100.38
KE59-2972	50.59	2.900	13.62	12.87	0.18	6.17	10.31	2.48	0.580	0.310	100.01
Pu‘u ‘Ō‘ō - Episode 60											
15-Mar-11	51.01	2.369	13.61	12.16	0.18	6.85	10.90	2.21	0.393	0.222	99.90
6-May-11	51.38	2.379	13.88	12.05	0.17	6.67	10.92	1.85	0.393	0.225	99.92
23-Jun-11	51.37	2.358	13.63	12.03	0.18	6.74	11.00	1.75	0.392	0.222	99.67
11-Aug-11	51.21	2.324	13.52	12.03	0.17	7.10	10.91	1.97	0.388	0.217	99.84
Standard											
BHVO-1	49.70	2.722	13.47	12.32	0.18	7.04	11.42	2.25	0.522	0.286	99.91
BHVO-1	49.78	2.723	13.33	12.32	0.18	6.99	11.41	2.22	0.522	0.285	99.76
BHVO-1	49.65	2.717	13.38	12.31	0.18	6.98	11.36	2.29	0.519	0.285	99.67
BHVO-1	49.81	2.727	13.49	12.29	0.18	7.02	11.48	2.28	0.531	0.287	100.10
BHVO-1	49.61	2.708	13.30	12.30	0.18	6.99	11.36	2.29	0.527	0.287	99.55
BHVO-1	49.75	2.721	13.44	12.31	0.18	7.03	11.43	2.25	0.522	0.287	99.92
BHVO-1	49.54	2.726	13.55	12.33	0.18	7.07	11.45	2.23	0.521	0.279	99.87
BHVO-1	49.50	2.724	13.46	12.31	0.18	7.09	11.41	2.23	0.521	0.280	99.70

BHVO-1	49.54	2.719	13.38	12.31	0.18	7.05	11.44	2.23	0.518	0.283	99.65
BHVO-1	49.45	2.722	13.48	12.31	0.17	7.01	11.42	2.23	0.517	0.280	99.60
BHVO-1	49.54	2.728	13.41	12.32	0.18	7.04	11.43	2.23	0.516	0.282	99.67
BHVO-1	49.57	2.721	13.54	12.30	0.17	7.12	11.42	2.23	0.520	0.281	99.88
BHVO-1	49.61	2.726	13.55	12.32	0.18	7.02	11.43	2.23	0.519	0.281	99.85
BHVO-1	49.56	2.725	13.45	12.32	0.18	6.96	11.44	2.23	0.522	0.281	99.67
BHVO-1	49.63	2.723	13.31	12.30	0.18	7.02	11.54	2.23	0.520	0.282	99.72
BHVO-1	49.60	2.716	13.49	12.29	0.18	7.09	11.50	2.23	0.519	0.282	99.89
BHVO-1	49.56	2.720	13.56	12.31	0.18	7.06	11.50	2.23	0.518	0.280	99.91
BHVO-1	49.60	2.720	13.49	12.30	0.18	7.10	11.52	2.23	0.521	0.277	99.92
BHVO-1	49.64	2.727	13.58	12.31	0.18	7.08	11.58	2.23	0.520	0.281	100.12
BHVO-1	49.60	2.722	13.56	12.29	0.18	7.07	11.54	2.23	0.522	0.283	99.99

Notes: Data for samples DAS69-3-2 and KI-77-13 from Pietruszka *et al.* (in preparation); episode 35 data are from Thornber *et al.* (2002); episodes 58 and 60 data are from M. Garcia (unpublished data). Episode 1 samples with (*,$^{+}$, or ^) represent samples that have higher-MgO compositions, hybrid compositions, or 1977-like compositions, respectively (Garcia *et al.*, 1992). See Appendix B for sample locations.

The XRF trace element data for the historical upper to middle ERZ fissure eruptions (Table 4) define overall collinear trends on incompatible element variation diagrams (e.g., Fig. 12a). When plotted against Ba (a highly incompatible element), Y, Rb, Nb, Zn, Sr, and V show positive trends; Cr shows a negative trend (Fig. 12b), and Ni shows no overall trend. Plots of Zn, Sr, Y, and V show considerable variation at the same Ba content (Table 4). The lavas from the 1960s have higher Ba, Ni, Rb, Nb, and Sr contents compared to the Puʻu ʻŌʻō cone lavas (episodes 58 and 60; Table 4). Lavas from the Puʻu ʻŌʻō cone (episodes 58 and 60) have lower Ti, Ba, Nb, Sr, and Zr than all other lavas. The more evolved episode 59 products have a higher Nb/Y (~0.63) than the less evolved episode 59 lavas (Nb/Y ~0.55; Fig. A1). Olivine, plagioclase, and/or clinopyroxene fractionation do not affect Nb/Y (Henderson, 1982), which makes this ratio a useful indicator of parental magma affinity.

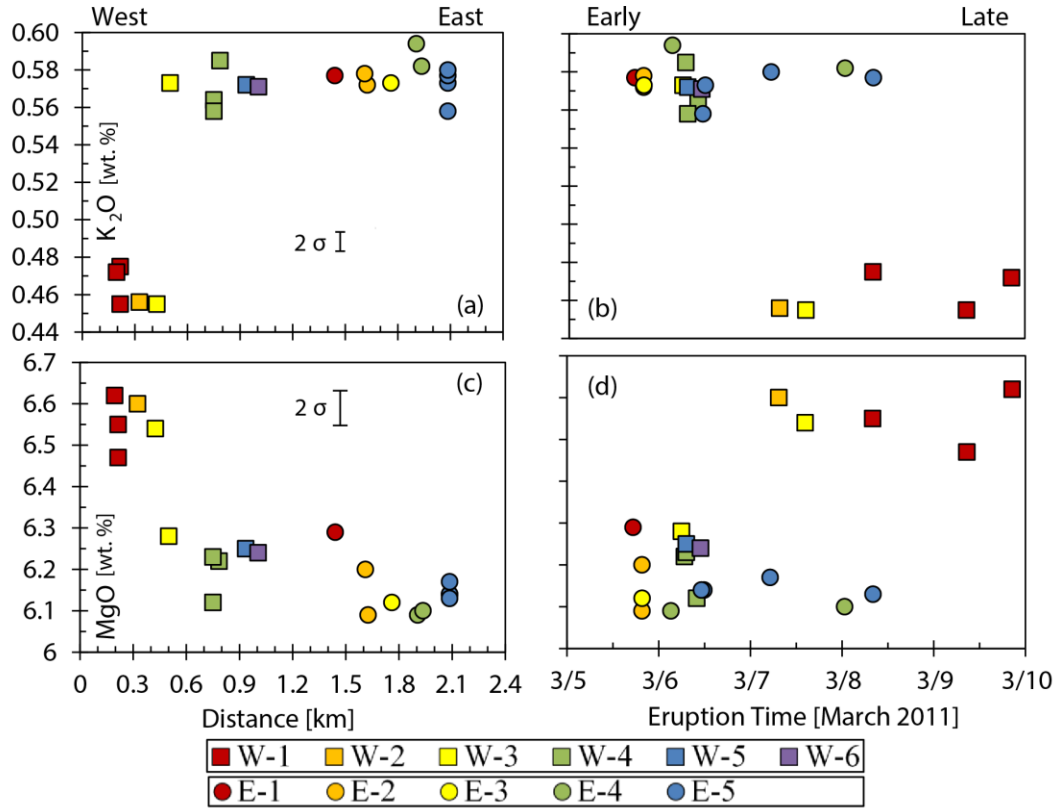

Fig. 11. Spatial, temporal, and geochemical relations of episode 59 lavas. Legend shows symbol for each vent. (a) K_2O variation with distance measured from Nāpau Crater's east rim. (b) K_2O variation with time of sample eruption. (c) MgO variation with distance measured from Nāpau Crater's east rim. (d) K_2O variation with time of sample eruption.

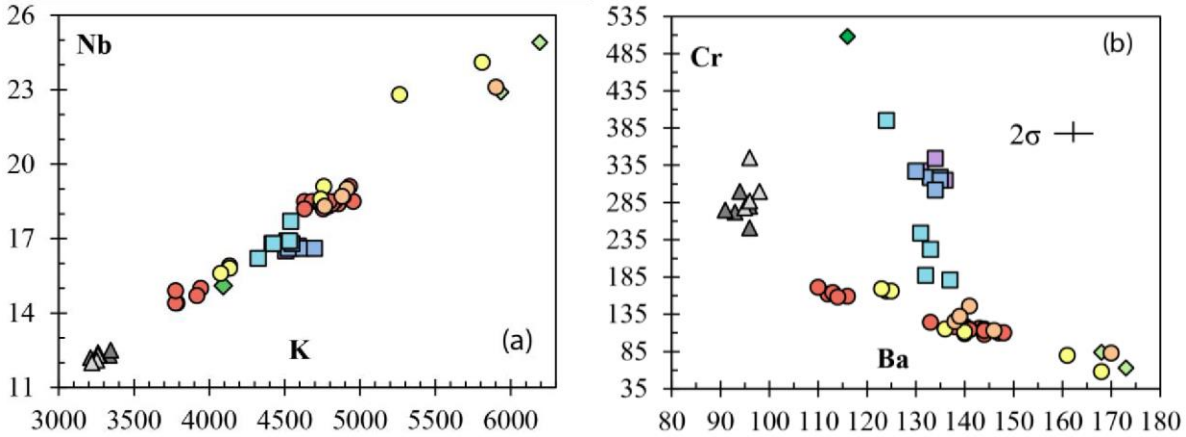

Fig. 12. Trace element variation diagrams for upper to middle ERZ lavas. Symbols as in Fig. 10. Data for samples DAS69-3-2 and KI-77-11 are from Pietruszka *et al.* (in preparation). Data for episodes 58 and 60 sourced from M. Garcia (unpublished data). (a) Nb vs. K variation. The 2σ error bars are within the size of the symbol. (b) Cr vs. Ba variation.

Table 4: XRF analyses of trace element concentrations (in ppm) for upper to middle ERZ samples.

Sample	Nb	Zr	Y	Sr	Rb	Zn	Ni	Cr	V	Ba
Pre-Puʻu ʻŌʻō										
KE1922-09	23.6	262	37.4	372	13.5	142	75	74	371	172
KE1922-08	17.1	185	26.1	390	10.0	120	79	155	309	131
KE1963-14	16.7	183	25.8	382	10.0	117	102	327	293	131
KE1963-04	16.5	181	25.1	382	9.4	117	108	344	292	134
KE1963-03	16.7	183	25.4	386	10.1	118	100	315	292	136
KE1963-02	16.6	183	25.7	388	9.6	119	102	319	291	133
KE1965-20	16.9	184	25.8	386	9.4	118	96	302	290	134
KE1965-34	16.6	183	24.8	391	9.9	117	97	319	288	135
KE1965-15	16.6	183	25.5	386	9.8	118	101	327	293	130
KE1965-17	16.6	181	25.1	387	10.0	116	99	319	285	133
KE1965-19	16.8	185	25.1	383	9.9	119	99	315	293	135
KE1968-35	16.9	181	25.7	390	9.7	119	84	187	300	132
KE1968-36	16.8	182	25.2	386	9.7	119	95	222	294	133
DAS69-3-2	15.1	161	23.2	353	8.2	118	197	508	274	116
KI-77-13	24.9	254	35.2	393	12.9	141	67	63	338	173
KI-77-11	22.9	239	32.6	405	12.6	133	70	84	324	168
Puʻu ʻŌʻō - Episode 1										
KE1983-13	15.6	172	26.4	364	8.8	117	89	169	303	123
KE1983-12	15.8	174	26.4	366	9.0	117	89	166	296	125
KE1983-11	15.9	174	26.6	364	8.9	119	89	166	303	124
KE1-53	19.1	196	28.2	388	10.1	124	80	111	319	140
KE1-58	18.6	193	27.8	386	9.6	123	82	115	309	136
KE1-38	24.1	236	32.5	404	12.6	136	67	58	342	168
KE1-25	22.8	227	31.5	399	12.1	131	72	80	331	161
Puʻu ʻŌʻō - Episode 54										
Vent F	23.1	242	33.5	394	12.9	136	69	83	354	170
Vent A	18.7	198	28.6	382	10.7	126	83	146	317	141
Vent B	19.0	201	28.8	387	10.9	136	78	113	319	146
Vent D	18.3	196	28.5	383	10.5	125	79	125	316	138
Vent E	18.7	199	28.6	383	10.7	125	80	132	319	139
Puʻu ʻŌʻō - Episode 58										
29-Sep-10	12.3	146	25.5	311	5.5	113	73	272	281	93
6-Oct-10	12.3	145	25.2	311	5.6	114	77	280	284	96
20-Nov-10	12.3	144	24.8	309	5.6	112	76	275	276	91
12-Jan-11	12.5	147	25.6	313	5.6	114	68	251	284	96
13-Feb-11	12.2	142	24.8	310	5.7	114	79	300	278	94
Puʻu ʻŌʻō - Episode 59										
KE59-2955	14.4	166	26.4	342	8.0	120	72	162	299	112
KE59-2958	15.0	171	26.9	346	8.3	120	73	159	299	116
KE59-2968	14.9	168	27.1	343	6.8	119	72	164	303	113
KE59-2980	14.7	169	26.7	344	8.4	120	73	158	298	114
KE59-2979	18.2	196	28.6	375	10.3	126	74	118	319	138
KE59-2942	18.4	197	28.8	378	10.4	126	74	116	323	143
KE59-2965	18.5	193	29.0	373	8.7	125	74	119	325	140
KE2011-33	18.2	196	28.8	376	10.1	125	75	124	311	133
KE59-2957	14.4	164	27.2	338	6.5	118	72	171	300	110
KE59-2964	18.4	197	28.7	377	10.5	126	72	121	318	139
KE59-2975	18.4	197	28.9	379	10.4	123	73	119	311	139

KE59-2952	18.3	197	28.7	378	10.3	127	74	117	324	139
KE59-2950	18.5	197	29.6	376	9.0	126	72	110	325	147
KE59-2974	18.5	198	28.8	382	10.4	123	73	114	311	141
KE59-2949	18.4	198	28.7	378	10.7	127	74	114	324	141
KE59-2947	19.1	205	29.7	380	10.6	128	73	108	328	144
KE59-2944	18.5	197	29.5	376	9.0	126	72	109	323	140
KE59-2960	18.5	199	29.8	376	8.9	126	71	110	321	148
KE59-2943	18.6	200	29.1	379	10.6	127	74	113	323	144
KE59-2959	18.5	197	29.5	375	9.0	125	72	115	320	144
KE59-2982	18.5	200	29.1	376	10.4	126	73	113	320	144
KE59-2972	18.4	199	29.0	378	10.5	124	73	115	310	141
Pu‘u ‘Ō‘ō - Episode 60										
15-Mar-11	12.4	144	24.9	311	5.7	113	75	278	279	95
6-May-11	12.3	143	24.9	308	5.7	115	77	287	276	96
23-Jun-11	12.1	143	24.7	309	5.5	118	81	300	285	98
11-Aug-11	12.0	141	24.5	307	5.5	115	93	345	285	96
Standard										
BHVO-1	18.7	176	25.2	381	9.2	112	115	298	296	130
BHVO-1	18.8	180	24.9	379	9.7	113	113	299	288	125
BHVO-1	18.5	174	25.1	379	9.2	112	114	297	297	132
BHVO-1	18.3	168	24.9	373	8.9	111	113	299	293	127
BHVO-1	18.6	174	25.3	381	9.2	112	114	297	294	135
BHVO-1	18.9	178	25.7	376	9.0	112	115	296	294	136
BHVO-1	19.0	178	25.7	377	8.8	113	115	297	291	133
BHVO-1	18.8	177	25.6	375	8.9	112	115	298	294	135
BHVO-1	19.0	178	25.7	377	8.8	113	115	297	291	133
BHVO-1	19.0	179	25.9	377	8.5	113	116	298	295	137
BHVO-1	19.0	179	26.1	378	8.3	113	116	300	294	135
BHVO-1	18.9	176	25.9	374	8.8	111	114	294	289	139
BHVO-1	18.9	176	25.8	375	8.7	112	115	297	290	137
BHVO-1	18.4	180	24.9	393	9.3	110	112	296	281	130
BHVO-1	18.4	179	24.6	378	9.2	111	112	294	284	125
BHVO-1	18.3	179	24.9	390	9.2	110	109	286	283	131
BHVO-1	18.4	179	24.6	378	9.3	111	112	294	287	131
BHVO-1	18.5	179	25.0	380	9.2	111	112	296	284	128
BHVO-1	18.6	180	25.0	382	9.1	112	112	296	286	133
BHVO-1	18.3	179	24.8	379	9.0	110	111	293	283	129
BHVO-1	18.4	179	24.6	378	9.2	111	112	294	284	125
BHVO-1	18.5	179	25.0	380	9.2	111	112	296	284	128
BHVO-1	18.4	180	24.9	393	9.3	110	112	296	281	130
BHVO-1	18.4	179	24.6	378	9.2	111	112	294	284	125
BHVO-1	18.3	179	24.9	390	9.2	110	109	286	283	131
BHVO-1	18.4	179	24.6	378	9.3	111	112	294	287	131
BHVO-1	18.5	179	25.0	380	9.2	111	112	296	284	128
BHVO-1	18.6	180	25.0	382	9.1	112	112	296	286	133

Notes: Data for samples DAS69-3-2 and KI-77-13 from Pietruszka *et al.* (in preparation); episodes 58 and 60 data are from M. Garcia (unpublished data). See Rhodes & Vollinger (2004) for a discussion of the methods used. See Appendix B for sample locations.

DISCUSSION

The petrological relationships of lavas from historical ERZ fissure eruptions are evaluated to better understand the spatial and temporal evolution of crustal magmatic processes that caused the geochemical variations seen in lavas from Nāpau Crater's most recent episode, the March 2011 eruption (episode 59). To provide context for the discussion, this section begins with a summary of petrogenesis at Kīlauea and provides a brief overview of the magmatic history of Pu‘u ‘Ō‘ō lavas that erupted in the Nāpau Crater area.

Petrogenesis at Kīlauea Volcano

Kīlauea's magma ascends from the upper mantle (~60 km, based on maximum earthquake depths) into the summit region of the volcano where it accumulates and mixes within a storage reservoir and/or is injected into the rift zones (e.g., Wright, 1971). Magma that is injected into and erupted from the rift zones is usually dominated by olivine-only fractionation (Wright, 1971). Intruded magma may accumulate in shallow (~1.6-3 km) 'pods' or 'pockets' along the rift zone where it continues to cool and fractionate (Wright & Fiske, 1971; Mittelstaedt & Garcia, 2007). This cooling magma becomes evolved (crystallizes olivine + clinopyroxene ± plagioclase) within the ERZ as it fractionates over time (Wright & Fiske, 1971). These magmas may interact with new injections of summit magma, forming hybrids (e.g., Garcia *et al.*, 1992; Orr *et al.*, 2015).

Examples of hybrid magmas formed by mixing of older, more evolved and newer, more MgO-rich magma includes episodes 1 and 54 of the Pu‘u ‘Ō‘ō eruption (Garcia *et al.*, 1989; Garcia *et al.*, 2000; Thornber *et al.*, 2003). Petrographic and geochemical evidence commonly attributed to magma mixing in ERZ lavas include (a) resorbed and/or reversely zoned minerals, (b) linear variations among all major and trace elements, (c) low residuals from least squares mixing calculations, (d) bimodal compositional ranges in olivine and/or plagioclase (e) and an abundance of phase compositions that are interpreted to be out of equilibrium with their host rock (e.g., Wright, 1971; Wright & Helz, 1996; Garcia *et al.*, 1989).

Episode 59 lavas were proposed to result from mixing between more MgO-rich dike magma and an older pod of stored magma that had undergone multigenerational magma hybridization (i.e. mixing among multiple previously emplaced magmas; Thornber *et al.*, 2015; Orr *et al.*, 2015). Altogether, this is the working baseline model for petrogenesis at Kīlauea and

for the source magmas of episode 59, yet the question, 'which magmas are the mixing end-members for episode 59 lavas?' remains unanswered. It has been suggested that fractionated episode 1 magma was a mixing component in episode 59 magma and that episode 1 products were themselves mixed with fractionated 1960s magma, based on the physical proximity and geochemical signature of lavas from the associated eruptions in the Nāpau Crater area (Thornber *et al.*, 2015). This hypothesis was not tested using least squares regression calculations.

Least squares regression calculations can identify or eliminate potential mixing end-members and provide insight into spatial and temporal geochemical variations. This study confirms magma mixing and proposes new potential mixing end-members based on trends in glass, whole-rock, and olivine analyses that are supported by least squares regression calculations.

Evidence of magma mixing prior to episode 59

Magma mixing in episode 59 lavas is indicated by reversely zoned olivine (Fig. 7) and clinopyroxene and sieve-textured plagioclase. Rounded (resorbed) crystals were not found in lavas from episode 59; however, reverse zoning was seen in 80% of the analyzed olivine profiles (Fig. 8). Reverse zoning (e.g., Fig. 7b) is the result of mixing with a more magnesian magma (e.g., Pearce, 1984). Episode 59 olivine cores from the less evolved batch show a bimodal Fo distribution (Fig. 6) indicating two geochemically distinct magmas were mixed. Olivine cores from lavas of the less evolved batch with >79% Fo contain NiO and Fo concentrations that are indistinguishable from those of olivine erupted from the Puʻu ʻŌʻō vent during episode 58 (Fig. 13). Thus, the episode 58 lavas are a potential lower-MgO end-member for episode 59 lavas (as suggested by Thornber *et al.* (2015) and Orr *et al.* (2015) based on their temporal association with episode 59). Most episode 59 olivine cores (70%) have Fo contents that are too low to be in equilibrium with a melt corresponding to their whole-rock composition (Fig. 6). In addition to a population of olivine that is bimodal, commonly reversely zoned, and typically out of equilibrium with its host melt, a history of magma mixing for these lavas is also supported by whole-rock major oxide and trace element data, which define overall collinear trends among episode 59 samples on all variation diagrams (e.g., Figs. 10 & 12).

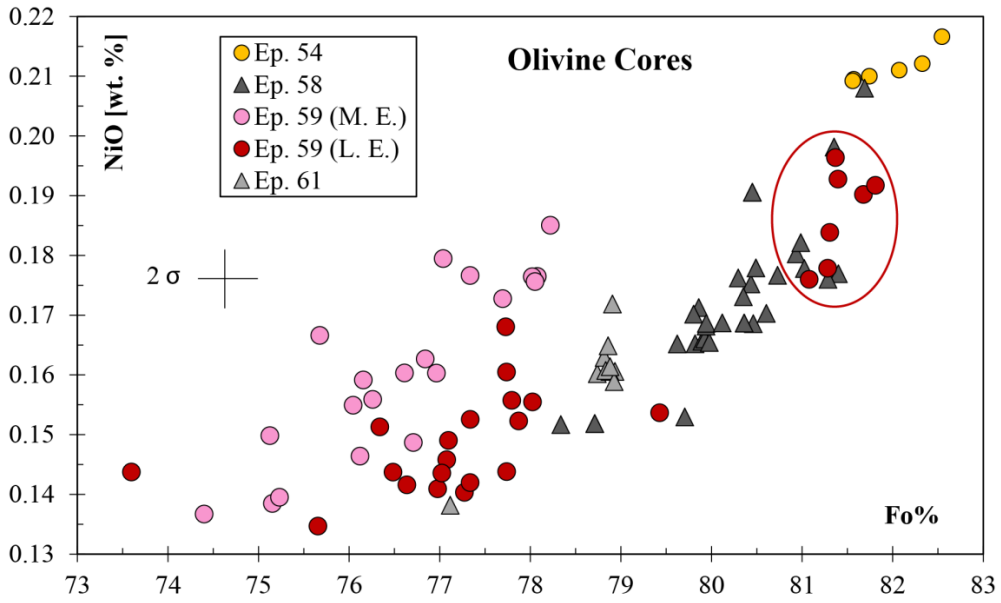

Fig. 13. Olivine core data for Pu‘u ‘Ō‘ō episodes 54, 58, 59, and 61. Data for episode 58 from Lynn *et al.* (2017) and Lynn *et al.* (unpublished data). Data from episode 61 from Lynn *et al.* (unpublished data). Red circle highlights episode 59 olivine crystals that are indistinguishable from episode 58 compositions erupted at the Pu‘u ‘Ō‘ō vent. In general, the episode 54 and more evolved episode 59 olivine cores have a higher NiO concentration than the less evolved olivine cores at a given Fo value. NiO and Fo contents in olivine cores reflect the compositions of the parental magmas that the olivine crystals grew in.

Episode 59 whole-rock compositions were proposed to fall on a mixing line between episode 58 and 60 compositions and the fractionated equivalents of samples from 1965, 1968, and episode 1 based on plots of Zr/Y vs. Nb/Y and MgO (Thornber *et al.*, 2015). This thesis modifies and expands the proposition: episode 59 whole-rock major-oxide compositions (those shown in Fig. 10) fall along mixing lines between samples from (a) 1977, (b) Pu‘u ‘Ō‘ō episodes 1, 54, 58 and 60, and/or (c) the fractionated equivalents of samples from 1963, 1965, 1968, 1969, and episode 1. Crystal fractionation trends (Fig. 10) were calculated for select samples using Petrolog (Danyushevsky & Plechov, 2011) since the compositions of actual differentiated stored magmas are unobtainable (i.e. they are located within the rift zone). These crystal fractionation trends are supported by glass compositions, which represent liquid lines of descent (Fig. 10). Several end-member compositions were tested to explain the compositions of episode 59 lavas using least squares regression and are discussed in the following section. Low residuals (<4σ analytical precision) for all major oxide and trace elements (except Cr) from successful trials offer further evidence in support of magma mixing (Tables 5-7).

Mixing end-members of episode 59 lavas

Potential mixing end-members for episode 59 were evaluated using the Igpet modeling program (Carr & Gazel, 2017), which uses least squares regression to calculate residuals from mixing two or more parent compositions as end-members for a given daughter composition. The residuals and sum of squares of residuals for SiO_2 and Al_2O_3 were weighted at 0.4 and 0.5, respectively, to reduce their dominance on the least squares solution. A mixing trial is considered successful (or end-members are considered viable) if each residual is $<4\sigma$ analytical precision.

Potential higher-MgO end-members

Pu‘u ‘Ō‘ō episodes 58 and 60 span a combined time range of about four years. Only Pu‘u ‘Ō‘ō data from within approximately six months before or after episode 59 were used in least squares modeling. The continuous flow of magma from the summit to Pu‘u ‘Ō‘ō and its eruption (Orr *et al.*, 2015) make it unlikely that a magma older or later resided within the main ERZ conduit. In each mixing calculation, a Pu‘u ‘Ō‘ō sample from either late episode 58 or early episode 60 was used as the more MgO-rich end-member.

Potential lower MgO end-members

The potential lower-MgO end-members of episode 59 lavas include whole-rock compositions from samples erupted in 1977 and Pu‘u ‘Ō‘ō episodes 1 and 54. Glass compositions of lava erupted in 1963, 1968, and during episodes 1 and 54 were also considered, and are interpreted to be representative of a fractionated residual magma stored in a shallow (~1.6-3 km deep) pod within the Nāpau Crater area. In addition to these whole-rock and glass compositions, the calculated compositions of fractionated 1963, 1965, 1968, and 1969 lavas were also tested as end-members of episode 59 lavas. Unfractionated compositions (i.e. whole-rock compositions) for 1960s and episode 35 lavas were not considered as a potential lower-MgO end-member for episode 59 lavas because they are not collinear with Pu‘u ‘Ō‘ō episode 58 or 60 samples.

End-members of the less evolved batch (later episode 59 lavas)

The average composition of the less evolved batch can be explained by binary mixing. Viable lower-MgO end-members for the less evolved batch include episode 58 samples (6-Oct-10, 20-Nov-10, and 13 Feb 11) and an episode 60 sample (15-Mar-11) from the Pu‘u ‘Ō‘ō vent. The episode 60 sample was collected just six days after episode 59 ended. A viable higher-MgO end-member is a fractionated episode 1 lava composition (represented by the glass composition of sample KE1983-12; Table 5).

Table 5: Least squares regression mixing calculation results for the less evolved batch of episode 59 lavas.

Ep. 59 Daughter Lava: Batch Average		Less Evolved			
Higher-MgO Parent *(sample)*		Ep. 60 *(15-Mar-11)*	Ep. 58 *(6-Oct-10)*	Ep. 58 *(20-Nov-10)*	Ep. 58 *(13-Feb-11)*
Lower-MgO Parent *(sample)*		Ep. 1 *(KE1983-12*)*	Ep. 1 *(KE1983-12*)*	Ep. 1 *(KE1983-12*)*	Ep. 1 *(KE1983-12*)*
	(4σ)	Major element residuals			
SiO_2^+	(± 0.36)	-0.07	-0.06	-0.07	-0.05
TiO_2	(± 0.02)	-0.01	-0.01	-0.01	-0.02
$Al_2O_3^+$	(± 0.35)	0.12	0.08	0.12	0.1
FeO	(± 0.05)	-0.01	0.00	-0.03	-0.03
MnO	(± 0.01)	0.01	0.01	0.01	0.01
MgO	(± 0.17)	0.04	0.03	0.01	-0.02
CaO	(± 0.24)	-0.11	-0.08	-0.09	-0.07
Na_2O	(± 0.09)	0.05	0.05	0.05	0.06
K_2O	(± 0.01)	0.00	0.00	0.00	-0.01
P_2O_5	(± 0.01)	0.01	0.01	0.01	0.01
Σ (r^2)		0.035	0.021	0.03	0.024
		Mixing Proportions			
%Higher-MgO Parent		64	63	63	60
%Lower-MgO Parent		36	37	37	40

Notes: *Indicates glass composition; trace element data not available for glass compositions. $^+$Indicates oxides with weighted value; SiO_2 and Al_2O_3 weighted by 0.4 and 0.5, respectively. XRF whole-rock compositions were used for episode 58 and 60 samples. The 4σ values were calculated from an average of analyses (n = 21) of the BHVO-1 standard that was ran with XRF analyses in Table 3.

End-members of the more evolved batch (earlier episode 59 lavas)

Unlike the less evolved batch, the average composition of the more evolved batch cannot be explained by simple binary mixing. No single lower-MgO end-member (when mixed with a single higher-MgO end-member) yielded sufficiently low residuals (<4σ analytical precision) in binary mixing calculations. Ternary mixing involving two lower-MgO end-members (and a single higher-MgO end-member), however, did produce successful results.

The average composition of the more evolved batch was successfully obtained by calculations that involved mixing between sample KE1-25 (from episode 1) and sample Vent A (from episode 54) as the two lower-MgO end-members and either sample 29-Sep-10 or 12-Jan-

11 (from episode 58) as the higher-MgO end-member. Similarly, using sample KE1-38 (from episode 1) and sample Vent A (from episode 54) as the two lower-MgO end-members and any of the five episode 58 samples or episode 60 sample 15-Mar-11 as the higher-MgO end-member had acceptably low residuals for major oxides and trace elements (Table 6). The mixing of magmas from episodes 1 and 54 to create the compositions seen in the more evolved batch of episode 59 lavas is a geologically feasible scenario. Episode 1, 54, and 59 lavas that erupted from episode 1, 54, and 59 fissures that are either overlapping or offset by <250 m have very similar whole-rock and glass compositions.

Table 6: Least squares regression mixing calculation results involving episode 1 and 54 parents for the more evolved batch of episode 59 lavas.

Ep. 59 Daughter Lava: Batch Average		More Evolved							
Higher-MgO Parent *(sample)*		Ep. 58 *(29-Sep-10)*	Ep. 58 *(12-Jan-11)*	Ep. 58 *(29-Sep-10)*	Ep. 58 *(6-Oct-10)*	Ep. 58 *(20-Nov-10)*	Ep. 58 *(12-Jan-11)*	Ep. 58 *(13-Feb-11)*	Ep. 60 *(15-Mar-11)*
Lower-MgO Parent 1 *(sample)*		Ep. 1 *(KE1-25)*	Ep. 1 *(KE1-25)*	Ep. 1 *(KE1-38)*	Ep. 1 *(KE1-38)*	Ep. 1 *(KE1-38)*	Ep. 1 *(KE1-38)*	Ep. 1 *(KE1-38)*	Ep. 1 *(KE1-38)*
Lower-MgO Parent 2 *(sample)*		Ep. 54 *(Vent A)*	Ep. 54 *(Vent A)*	Ep. 54 *(Vent A)*	Ep. 54 *(Vent A)*	Ep. 54 *(Vent A)*	Ep. 54 *(Vent A)*	Ep. 54 *(Vent A)*	Ep. 54 *(Vent A)*
	(4 σ)	Major element residuals							
SiO_2^+	(± 0.36)	-0.02	-0.03	-0.02	-0.03	-0.04	-0.03	-0.03	-0.04
TiO_2	(± 0.02)	-0.02	-0.02	0.00	0.01	0.01	0.01	0.00	0.01
$Al_2O_3^+$	(± 0.35)	0.04	0.04	0.04	0.03	0.05	0.03	0.04	0.05
FeO	(± 0.05)	0.01	0.01	-0.03	-0.02	-0.03	-0.02	-0.03	-0.02
MnO	(± 0.01)	-0.01	0.00	0.00	0.00	0.00	0.00	0.00	0.00
MgO	(± 0.17)	-0.02	-0.03	-0.01	-0.06	-0.07	-0.02	-0.08	-0.06
CaO	(± 0.24)	0.01	0.02	-0.01	0.07	0.06	0.02	0.08	0.05
Na_2O	(± 0.09)	0.02	0.02	0.05	0.03	0.03	0.04	0.03	0.03
K_2O	(± 0.01)	0.00	0.00	0.00	0.00	0.00	0.00	0.00	0.00
P_2O_5	(± 0.01)	-0.01	-0.01	-0.01	0.00	0.00	0.00	-0.01	0.00
Σ (r^2)		0.004	0.004	0.005	0.012	0.015	0.005	0.018	0.011
		Trace Element Residuals							
Rb	(± 1.1)	-0.4	-0.4	0.0	0.1	0.1	0.1	0.0	0.1
Sr	(± 21.1)	0.1	0.7	5.9	8.5	9.0	7.0	7.7	8.5
Ba	(± 15.8)	0.0	0.0	3.4	2.8	4.3	3.5	2.5	3.2
Y	(± 1.8)	-0.3	-0.3	-0.2	-0.3	-0.1	-0.2	-0.3	-0.1
Zr	(± 10.3)	-4.2	-3.7	-0.5	-0.4	-0.3	0.3	-0.8	0.0
Nb	(± 1.0)	-1.0	-0.9	-0.5	-0.7	-0.7	-0.5	-0.8	-0.7
Ni	(± 7.4)	-3.1	-2.0	-1.2	-0.4	0.0	0.6	-0.7	0.2
V	(± 19.8)	2.7	2.6	2.6	1.7	4.4	2.6	2.8	3.5
Cr	(± 12.8)	**-24.4**	**-21.8**	**-33.8**	**-35.7**	**-33.0**	**-29.9**	**-39.3**	**-35.0**
		Mixing Proportions							
%Higher-MgO Parent		19	20	28	34	34	30	33	34
%Lower-MgO Parent 1		46	46	38	47	48	38	50	47
% Lower-MgO Parent 2		35	34	34	18	19	32	17	20

Notes: $^+$Indicates oxides with weighted value; SiO_2 and Al_2O_3 weighted by 0.4 and 0.5, respectively. XRF whole-rock major oxide and trace element compositions were used for each sample. The 4σ values were calculated from an average of analyses (n = 21 for major oxides, n = 28 for trace elements) of the BHVO-1 standard that was ran with XRF analyses in Tables 3 and 4.

Another viable model for the more evolved episode 59 batch involved mixing between episode 54 sample Vent A and 1977 sample KI-77-11 as the lower-MgO end-members and any of the five episode 58 samples or episode 60 sample 15-Mar-11 as the higher-MgO end-member (Table 7). Lavas from episode 1 are thought to have been mixed with a magmatic component that matched the composition of 1977 lava to create a hybrid magma that was erupted east of Nāpau Crater during episode 1 (Garcia *et al.*, 1989). The results from successful least-squares mixing calculations for the more evolved episode 59 batch show that episode 1 samples can be replaced by a sample from the 1977 eruption. This is consistent with the hypothesis that episode 1 samples that erupted east of Nāpau Crater contained a component of 1977-like magma.

Mixing calculations involving whole-rock, glass, or fractionated equivalents (as calculated by Petrolog) of lavas from the 1960s resulted in unacceptably large residuals ($\geq 4\sigma$ analytical precision) and thus cannot be a mixing component for either batch of episode 59 lavas (Table 8). This result is contrary to a previous hypothesis, which proposed that fractionated 1960s dike residua and fractionated hybrid episode 1 magmas (made up of more MgO-rich rift-conduit magma and fractionated 1960s dike residua) were a component in episode 59 lavas (Thornber *et al.*, 2015).

Table 7: Least squares regression mixing calculation results involving 1977 and episode 54 parents for the more evolved batch of episode 59 lavas.

Ep. 59 Daughter Lava: Batch Average		More Evolved					
Higher-MgO Parent *(sample)*		Ep. 58 *(29-Sep-10)*	Ep. 58 *(6-Oct-10)*	Ep. 58 *(20-Nov-10)*	Ep. 58 *(12-Jan-11)*	Ep. 58 *(13-Feb-11)*	Ep. 60 *(15-Mar-11)*
Lower-MgO Parent 1 *(sample)*		1977 *(KI-77-11)*	1977 *(KI-77-11)*	1977 *(KI-77-11)*	1977 *(KI-77-11)*	1977 *(KI-77-11)*	1977 *(KI-77-11)*
Lower-MgO Parent 2 *(sample)*		Ep. 54 *(Vent A)*	Ep. 54 *(Vent A)*	Ep. 54 *(Vent A)*	Ep. 54 *(Vent A)*	Ep. 54 *(Vent A)*	Ep. 54 *(Vent A)*
	(4 σ)	Major element residuals					
SiO_2^+	(± 0.36)	-0.03	-0.03	-0.03	-0.03	-0.02	-0.03
TiO_2	(± 0.02)	-0.02	-0.02	-0.02	-0.02	-0.02	-0.02
$Al_2O_3^+$	(± 0.35)	0.04	0.03	0.04	0.03	0.04	0.04
FeO	(± 0.05)	0.01	0.01	0.01	0.01	0.00	0.01
MnO	(± 0.01)	-0.01	0.00	0.00	0.00	-0.01	0.00
MgO	(± 0.17)	-0.02	-0.07	-0.07	-0.03	-0.08	-0.06
CaO	(± 0.24)	0.01	0.07	0.07	0.04	0.08	0.06
Na_2O	(± 0.09)	0.04	0.03	0.03	0.04	0.03	0.03
K_2O	(± 0.01)	-0.01	-0.01	-0.01	-0.01	-0.02	-0.01
P_2O_5	(± 0.01)	-0.01	-0.01	-0.01	0.00	-0.01	-0.01
$\Sigma (r^2)$		0.005	0.013	0.015	0.006	0.017	0.012
		Trace Element Residuals					
Rb	(± 1.1)	-0.1	-0.2	-0.2	-0.1	-0.3	-0.2
Sr	(± 21.1)	7.2	7.7	8.3	7.6	7.0	8.1
Ba	(± 15.8)	2.8	1.7	2.8	2.8	1.4	2.1
Y	(± 1.8)	-0.6	-0.6	-0.6	-0.5	-0.6	-0.6
Zr	(± 10.3)	-3.1	-3.9	-3.8	-2.5	-4.4	-3.5
Nb	(± 1.0)	-0.4	-0.5	-0.5	-0.4	-0.6	-0.5
Ni	(± 7.4)	-4.0	-4.4	-4.0	-2.8	-4.7	-3.8
V	(± 19.8)	4.7	3.9	5.8	4.6	4.6	5.3
Cr	(± 12.8)	-39.4	-39.9	-38.2	-36.0	-42.2	39.8
		Mixing Proportions					
%Higher-MgO Parent		22	23	23	23	22	23
%Lower-MgO Parent 1		25	28	28	24	29	28
% Lower-MgO Parent 2		53	50	49	53	50	49

Notes: $^+$Indicates oxides with weighted value; SiO_2 and Al_2O_3 weighted by 0.4 and 0.5, respectively. XRF whole-rock major oxide and trace element compositions were used for each sample. The 4σ values were calculated from an average of analyses (n = 21 for major oxides, n = 28 for trace elements) of the BHVO-1 standard that was ran with XRF analyses in Tables 3 and 4.

Table 8: Representative examples of least squares regression mixing calculation results for episode 59 lavas involving calculated fractionated compositions of 1960s magma.

Ep. 59 Daughter Lava: Batch Average		Less Evolved	More Evolved	More Evolved	More Evolved
Higher-MgO Parent *(sample)*		Ep. 60 *(15-Mar-11)*	Ep. 60 *(15-Mar-11)*	Ep. 58 *(29-Sep-10)*	Ep. 58 *(29-Sep-10)*
Lower-MgO Parent *(sample)*		1968‡ *(fractionate at 5.75 MgO)*	1968‡ *(fractionate at 5.75 MgO)*	1963‡ *(fractionate at 6.15 MgO)*	1965‡ *(fractionate at 6.15 MgO)*
	(4σ)	Major element residuals			
SiO_2^+	(± 0.36)	-0.02	0.00	0.03	0.05
TiO_2	(± 0.02)	**0.09**	**0.24**	**0.27**	**0.28**
$Al_2O_3^+$	(± 0.35)	0.13	0.18	0.19	0.19
FeO	(± 0.05)	**-0.11**	**-0.29**	**-0.20**	**-0.17**
MnO	(± 0.01)	-0.01	-0.01	-0.01	-0.01
MgO	(± 0.17)	-0.11	**-0.33**	**-0.17**	**-0.18**
CaO	(± 0.24)	-0.19	**-0.35**	**-0.63**	**-0.67**
Na_2O	(± 0.09)	**0.10**	**0.28**	**0.24**	**0.20**
K_2O	(± 0.01)	**0.03**	**0.10**	**0.09**	**0.08**
P_2O_5	(± 0.01)	**0.02**	**0.05**	**0.04**	**0.04**
Σ (r^2)		0.098	0.496	0.64	0.678
		Mixing Proportions			
%Higher-MgO Parent		85	70	59	60
%Lower-MgO Parent		15	30	41	40

Notes: +Indicates oxides with weighted value; SiO_2 and Al_2O_3 weighted by 0.4 and 0.5, respectively. ‡Indicates a calculated fractionated composition that is collinear (on Fig. 10a) with either sample 15-Mar-11 or 29-Sep-10 and the average composition of an episode 59 batch; trace element data not available for calculated fractionate compositions. XRF whole-rock compositions were used for episode 58 and 60 samples. 4σ values were calculated from an average of analyses (n = 21) of the BHVO-1 standard that was ran with XRF analyses in Table 3. Bold numbers indicate the residual is ≥4σ.

Spatial and temporal geochemical variations

The systematic sampling of lavas from episode 59 and 20th century historical Nāpau Crater area eruptions (Figs. 4 & 10) allows for interpretations of geochemical variations in space and time. Episode 59 samples were collected from each of the 11 vents and, on average, within <5 hours of each other for the entire duration of the 4.2-day-long eruption (Orr *et al.*, 2015). Samples with more evolved compositions were the first products erupted from episode 59 vents (Fig. 4). These samples were erupted sporadically between vents W-3 and E-5 for ~1.6 days until the evening of

March 6th, when less evolved compositions began to erupt (Fig. 4). Intermittent activity continued to issue lavas from both compositions for ~1.4 days; the more evolved samples erupted from vents E-4 and -5 while the less evolved samples came from vents W-1, -2, and -3 (Fig. 4). On the afternoon of March 8th, vents E-4 and -5 ceased to erupt and activity localized at vent W-1. Less evolved samples were erupted for the last ~1.3 days of episode 59 (Fig. 4).

Spatial and temporal variations of episode 59 lavas have been attributed to stored pockets of residual magma from 1960s eruptions mixing with and being progressively displaced by new magma diverted from Puʻu ʻŌʻō through an uprift breach in the ERZ conduit (Thornber *et al.*, 2015). This interpretation was based on plots of whole-rock MgO and Zr/Y against time. This interpretation is inconsistent with the results from least squares mixing calculations, which yielded unacceptably high residuals when glass, whole-rock, or calculated fractionated compositions from 1960s samples were tested as an end-member for episode 59 lavas. The change in proportions of end-members for each batch average provides insight into the temporal extent of mixing during episode 59. The percentage of more magnesian rift-conduit magma increased from 26% in the more evolved batch to 63% in the less evolved batch, on average (Tables 5-7). This is interpreted as an increase of fresh summit-derived magma replacing and mixing with pods of residual magma from episodes 1 and 54.

Forsterite concentration gradients were modeled using DIPRA (Girona & Costa, 2013), which solves the one-dimensional diffusion equation to retrieve timescales associated with a magmatic process. Each Fo profile was modeled as if it were oriented perpendicular to the c-axis. This approach provides a minimum timescale of storage after mixing because the diffusivity of Fe-Mg is approximately six times faster along the c-axis compared to the a- and b-axes (Dohmen & Chakraborty 2007). Each model was run at a pressure of 0.5 GPa and an oxygen fugacity of NNO -0.72 (Appendix E).

Modeling of Fo zoning patterns in olivine from both batches indicates that these two distinct batches of magma mixed with more magnesian, summit-diverted, rift-conduit magma for ~37-65 hours before the sample was erupted (Appendix E). This is based on results from an average of four diffusion models (Appendix E) and represents the amount of time that stored olivine crystals diffusively re-equilibrated to the more MgO-rich incoming melt before eruption. This result is consistent with seismic data, which suggests that the dike initiated ~3.5 hours before it breached the surface (Orr *et al.*, 2015). Adding 3.5 hours to the field-observed time of

eruption after episode 59 began (Fig. 4; Appendix A), samples used in the timescale modeling erupted between 21 and 69 hours after the dike began propagating (Appendix A). This timescale aligns well with the modeled timescale calculated using DIPRA (Appendix E).

Implications for Nāpau Crater magmas

Geophysical and geochemical constraints

Field, geophysical, and geochemical evidence are used here to constrain the sequence of events that led to the mixing of magma during episode 59. Field observations and geophysical data provide the inferred locations of intrusions and eruptions in the Nāpau Crater area during the prolonged Pu‘u ‘Ō‘ō eruption (e.g., Wolfe *et al.*, 1987; Owen *et al.*, 2000, Orr *et al.*, 2015). The pods of residual magma from previous intrusions under the Nāpau Crater area are probably above the ~3 km deep ERZ conduit feeding the Pu‘u ‘Ō‘ō eruption (e.g., Garcia *et al.*, 2000; Thornber *et al.*, 2015) and are most likely below ~1.6 km, based on the steep geothermal gradient above this depth, which promotes solidification (Mittelstaedt & Garcia, 2007). Volume estimates of intruded magma (23×10^6 m^3) and erupted lava (0.3×10^6 m^3) during episode 54 (Owen *et al.*, 2000) suggest that only about 1% of the intruded magma was erupted. The low residuals from least squares mixing calculations (those that involve episodes 1 and 54 lavas as the higher-MgO end-members for episode 59 lavas) are consistent with the pods under the Nāpau Crater area being able to remain in a molten state for decades (~28 years for episode 1, ~14 years for episode 54).

The presence of pods of residual magma (rather than a single reservoir) beneath the Nāpau Crater area is supported by the distinct geochemical ‘thumbprints’ of lavas from episodes 1, 54, and 59, which have different compositions (e.g., Fig. 10 & 13) spatially. For example, the initial episode 1 lavas (samples in Fig. 10a with black arrows stemming from them) that erupted in the northern edge of Nāpau Crater (Fig. 2) are less evolved than the other episode 1 lavas and did not show signs of mixing (Garcia *et al.*, 1989). Episode 1 fissures east of Nāpau Crater, however, erupted lavas with obvious magma mixing (e.g., resorbed and reversely zoned minerals, linear variations on all major and trace elements, low residuals for least squares mixing calculations) and became progressively more evolved (more like the compositions seen in 1977 lavas) with time (Garcia *et al.*, 1989). Furthermore, the episode 54 lavas are relatively homogenous geochemically (ranging from 6.2 - 6.4 wt. % MgO and 0.57 - 0.59 wt. % K_2O; Fig.

10a) except for lava from vent F (Fig. 2), which erupted much more evolved compositions (Fig. 10a) than those from vents A-E. Like episodes 1 and 54, fissures from episode 59 erupted lavas with distinct geochemical compositions from other lavas that were erupted within the same episode. This is an unlikely series of events if the Nāpau Crater area was underlain by a shallow magma reservoir (as suggested by Okamura *et al.*, 1988), which would lead to the homogenization of any intruded magma over time. Although the locations and interactions between magma pods under the Nāpau Crater area are unknown, geochemical and petrologic investigations offer insights to approximate locations and compositions.

Differences in whole-rock trace element geochemistry between episode 1 and 54 lavas have been attributed to each episode being sourced from compositionally distinct magmas (Garcia *et al.*, 2000). Fractionated incompatible element compositions of episode 1 lava (which could represent the composition of residual episode 1 magma) were dismissed as a mixing component for the hybrid compositions of episode 54 lava because they did not fall on a binary mixing line between episode 54 samples and a more MgO-rich episode 53 lava from Puʻu ʻŌʻō (Thornber *et al.*, 2003). Re-analyzed samples from episode 1 and 54 (Tables 3, 4, & A4) are not consistent with these conclusions. Instead, the data (Figs. 9, 10, & 12) are consistent with episode 54 vents A-E erupting lavas with compositions that closely match those that erupted in the same area during episode 1. The reason for this change in interpretations is most likely due to the improvement of trace element analytical error associated with XRF analyses. Samples KE1-53 (from episode 1) and Vent E (from episode 54) have nearly identical trace element concentrations (Table 4) and they erupted from vents just 80 m apart (Fig. 2). Similarly, the glass compositions for samples collected from several episode 1 vents located ≤2 km east of Nāpau Crater (Fig. 2) are similar geochemically to those from episode 54 vents A-E (Appendix C; Fig. 9). These observations, in addition to results from least squares modeling (Table 6), suggest that a hybrid pod of mixed, relatively unfractionated episode 1 and episode 54 magma was stored in the rift zone below the Nāpau Crater area before episode 59.

This pod of hybrid magma was intersected by a conduit-breaching dike just prior to episode 59 (Orr *et al.*, 2015). Whole-rock and glass compositional data for lavas from the more evolved batch (which were the first products of the eruption) show that they closely resemble episode 1 samples KE1-53 and -58 and episode 54 samples Vent A, B, D, and E (Tables 3, 4, & A4). Lavas from the less evolved batch, however, have a distinct geochemistry than the first

products of episode 59 (e.g., Fig. 11b). Acceptably low residuals (<4σ analytical precision) found for the evolved end-member of the less evolved batch were from binary mixing with the glass sample KE1983-12, which erupted in the northern edge of Nāpau Crater (Fig. 2). Mixing calculations involving whole-rock or glass compositions from episode 54 lavas resulted in unsatisfactory residuals. The episode 1 lavas that erupted in the north edge of Nāpau Crater were fed by a more magnesian source that was compositionally distinct from the more evolved episode 1 lavas that subsequently erupted just east of Nāpau Crater (Garcia *et al.*, 1989). The compositional and spatial difference between the initial and subsequent episode 1 lavas suggests a physical separation between these two pods within the rift (Fig. 14).

Sometime after episode 54 ended and before episode 59 began, the less evolved pod beneath Nāpau Crater contained a fractionated equivalent of the relatively more magnesian magma that fed the fissures in the north edge of Nāpau at the start of the episode 1. The other pod (farther east of Nāpau Crater) contained a mixture of hybrid episode 1 and 54 magmas. This eastern pod may have experienced a lesser extent of crystal fractionation than the more MgO-rich pod just west of it because mixing calculations using only lava compositions (rather than glass compositions, which represent a fractionated equivalent of the lava) yielded satisfactory residuals.

Synopsis of the episode 59 magma mixing scenario

Seismic and geodetic evidence indicates magma was diverted from the main ERZ conduit and intruded under the Nāpau Crater area (Lundgren *et al.*, 2013; Orr *et al.*, 2015). The dike apparently intersected two chemically distinct pods of previously intruded rift-zone-stored magma. The eastern pod contained a hybrid of seemingly unfractionated residual magma from Pu‘u ‘Ō‘ō episodes 1 and 54 that mixed with the intruding dike during episode 59 creating the more evolved batch of episode 59 lavas (Fig. 14). The western pod, under Nāpau Crater, was presumably tapped as the dike volume increased from an estimated 15×10^6 m^3 to 16×10^6 m^3 within the first day of the eruption (Lundgren *et al.*, 2013). This is consistent with the first lava sample from the less evolved batch (which originated from the newly tapped western pod) being collected 1.5 days after the start of the eruption. During the following 1.4 days, eruptive activity localized near the opposing ends of the western and eastern fissure systems, erupting lava from the less evolved and more evolved batch, respectively (Figs. 4 & 11b). The cessation of fountaining from the eastern vents on the afternoon of March 8th is the result of decreased

magmatic overpressure in that region (Orr *et al.*, 2015). After the eastern vents shut down, no evidence of lavas from the more evolved batch was subsequently detected. Only magma that mixed with the western pod supplied the remainder of the eruption at vents W-1 and W-2. Intrusion and eruption volumes were estimated to be 15.6×10^6 m^3 and 2.7×10^6 m^3, respectively (dense-rock equivalent, Lundgren *et al.*, 2013). This suggests that ~83% of the intruded magma during episode 59 still resides in pods beneath the Nāpau Crater area.

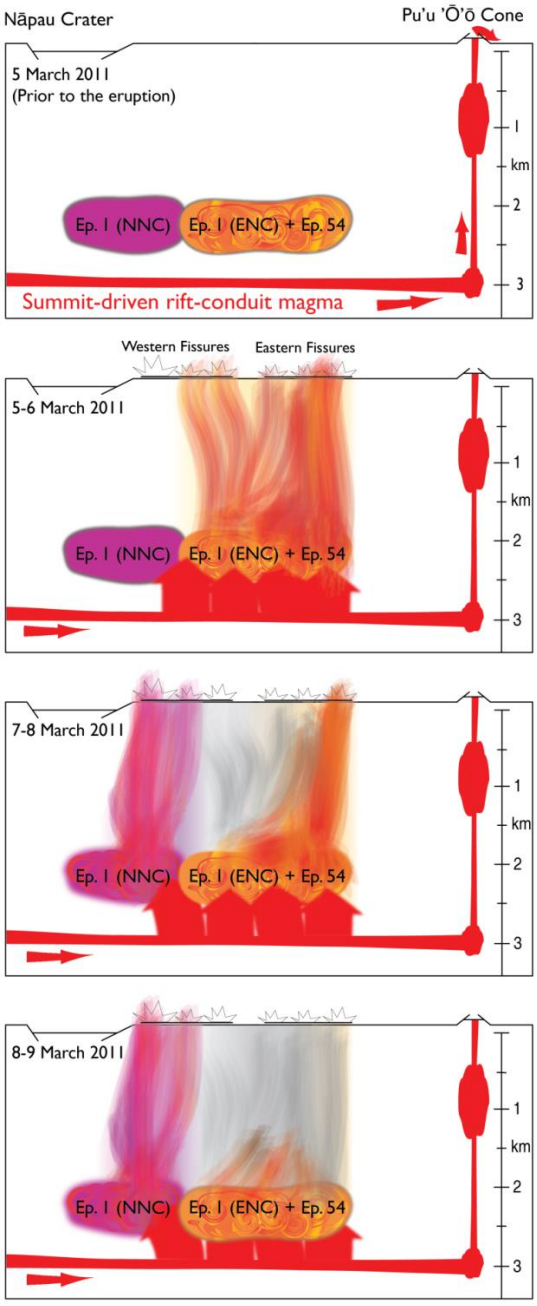

Fig. 14. Schematic of the sequence for producing the mixed magma erupted during episode 59. Abbreviations: NNC, North Nāpau Crater; ENC, East Nāpau Crater.

CONCLUSIONS

The petrography and geochemistry of lavas from episode 59 of the ongoing Pu‘u ‘Ō‘ō eruption at Kīlauea Volcano provide insights into the chemical compositions and locations of shallowly (~1.6-3 km deep) stored magmas in one of the most frequently active portions of the ERZ. Petrographic and geochemical investigations show that crystal fractionation and magma mixing were the dominant crustal processes that controlled episode 59 lava compositions. Evidence for crystal fractionation is evident from the assemblage of mineral phases (olivine + clinopyroxene + plagioclase) in episode 59 lavas. Fractionation beyond olivine controlled compositions occurred during decades of storage in pods of previously intruded magma. Petrologic evidence for mineral-melt disequilibrium in episode 59 lavas caused by magma mixing includes:

- reversely zoned olivine and clinopyroxene
- sieved-textured plagioclase
- bimodal Fo ranges in olivine cores (for the less evolved lavas)
- and a majority of olivine cores that are out of equilibrium with their host rock.

XRF analyses of whole-rock major oxide concentrations reveal two geochemically distinct magma batches for episode 59 that are collinear on all major oxide and trace element variation diagrams. The first batch erupted earlier and is more evolved (6.5-6.6 wt. % MgO) than the second batch (6.1-6.3 wt. % MgO), which mainly erupted later, although there is some overlap (Fig. 4). The more evolved batch mostly erupted from vents W-4 to E-5 whereas the less evolved batch predominantly erupted from the two westernmost vents, W-1 and W-2. Incompatible element plots (e.g., Nb vs. K, Nb/Y vs. Ba) indicate two different magma sources for episode 59 lavas.

The glass and whole-rock geochemistry of lavas from several other historical upper to middle ERZ fissure eruptions were determined to evaluate the mixing end-members for each batch of episode 59 lavas. Successful least squares mixing calculations (those with residuals $<4\sigma$ analytical precision) are consistent with the following:

- The less evolved batch is the result of binary mixing between magmas with compositions similar to (a) either an episode 58 or 60 sample, which erupted from a Pu‘u ‘Ō‘ō vent, and (b) an episode 1 glass sample KE1983-12, which erupted in the northern edge of Nāpau Crater.

- The more evolved batch is the result of ternary mixing among magmas with compositions similar to (a) either an episode 58 or 60 sample, which erupted from a Pu‘u ‘Ō‘ō vent, (b) an episode 54 sample, which erupted from vent A in Nāpau Crater, and (c) either an episode 1 sample that erupted ~3 km east of episode 59 vent E-5 or a 1977 sample, which is thought to have been a mixing component in hybrid episode 1 lavas.

The results herein suggest that these two physically and chemically distinct batches of stored residual magma were intersected by and mixed with more magnesian, summit-derived magma (with compositions similar to those seen in episode 58 and 60 lavas) before and during episode 59. Modeling of olivine zoning patterns indicates a minimum timescale of storage after mixing to be ~37-65 h. Episode 59 lavas with either more evolved or less evolved compositions originated from a more evolved or less evolved pod of magma, respectively (Appendix A; Fig. 14). Magma in the more evolved pod was most likely a hybrid of compositions similar to episode 1 lavas from vents east of Nāpau Crater and episode 54 lavas from vents A-E. Magma stored in the less evolved pod may have been the fractionated equivalent of magma that once fed the initial episode 1 fissures in the northern edge of Nāpau Crater.

The exact locations of magma storage pods under the Nāpau Crater area are unknown. This study offers clues to approximate sites and compositions. The probable locations of each pod (Fig. 14) were constrained by considering where its lavas were erupted. Thus, the more evolved pod containing a hybrid of episode 1 and 54 magmas may have been located beneath the segment of the rift just east of Nāpau Crater, where episode 1, 54, and 59 fissures are adjacent to each other (Fig. 2). The less evolved pod was probably located beneath vents W-1 through W-3, but also may extend slightly more west directly underneath Nāpau Crater, nearer to the episode 1 fissures that erupted in Nāpau Crater’s northern edge.

Petrologic insights gained from research on the lavas produced during episode 59 (which involved a significant change to the ERZ’s magmatic system during the sustained Pu‘u ‘Ō‘ō eruption) are important for assessing a Kīlauea’s magmatic behavior, which plays a role in evaluating its potential future activity. Based on the repeated nature of intrusions and eruptions in this region (ten within one century), the Nāpau Crater area serves as a magma depot within the ERZ. The chemically distinct batches of lavas that erupt from various locations in this area suggest that intruding dikes are likely to encounter and mix with pods of older, fractionated

residual magmas injected from previous intrusions rather than a single, homogenous reservoir of stored magma.

APPENDIX A

Episode 59 sample descriptions and batch associations including field-observed sample formation time and vent.

Sample	Site Description	Sample Description	Sample Formation Date	Batch
KE59-2958	W-1 (main vent)	Active phh overflow (spatter-fed) from ponded flow	3/8/11 8:00	L.E.
KE59-2968	W-1 (main vent)	Active phh overflow (spatter-fed) from ponded flow	3/9/11 8:38	L.E.
KE59-2980	W-1	Cold spatter from pond surface; last lava to erupt	3/9/11 20:30	L.E.
KE59-2955	W-2	Active phh flow (spatter-fed)	3/7/11 7:25	L.E.
KE59-2957	W-3(flow fed from west end)	Active phh overflow from ponded flow	3/7/11 14:20	L.E.
KE59-2979	W-3 (central portion)	Cold spatter; initial opening	3/6/11 5:57	M.E.
KE2011-33	W-4	Cold spatter collected in May, 2016	unknown	M.E.
KE59-2965	W-4 (main vent; on flow top)	Cold spatter	3/6/11 9:56	M.E.
KE59-2942	W-4 (main vent near east end)	Active phh flow (spatter-fed)	3/6/11 6:43	M.E.
KE59-2964	W-5 (east end)	Cold spatter	3/6/11 7:13	M.E.
KE59-2975	W-6 (main vent)	Cold phh	3/6/11 10:55	M.E.
KE59-2952	E-1 (west end)	Cold spatter	3/5/11 17:16	M.E.
KE59-2974	E-2 (main vent)	Cold (spatter-fed) phh flow	3/5/11 19:36	M.E.
KE59-2950	E-2 (east end)	Cold spatter	3/5/11 19:36	M.E.
KE59-2949	E-3 (east end)	Cold spatter	3/5/11 19:39	M.E.
KE59-2947	E-4 (central portion)	Warm spatter	3/6/11 3:10	M.E.
KE59-2960	E-4 (central portion)	Warm spatter from new vent	3/8/11 0:40	M.E.
KE59-2943	E-5 (main vent on west end)	Active phh flow (spatter-fed)	3/6/11 11:50	M.E.
KE59-2944	E-5 (main vent on west end)	Warm spatter	3/6/11 11:11	M.E.
KE59-2959	E-5 (main vent on west end)	Active phh from spatter-fed flow	3/8/11 8:05	M.E.
KE59-2972	E-5 (main vent at west end)	Cold pond surface phh fragment	3/7/11 5:10	M.E.
KE59-2982	E-5 (main cone/vent)	Cold spatter on top of last flow	3/8/11 11:15	M.E.

Notes: Field and sample notes from T. Orr (pers. comm.), except for sample KE2011-33. Abbreviations: W, west; E, east; phh, pāhoehoe; M.E., more evolved; L.E., less evolved. Samples ordered from westernmost to easternmost vent location.

APPENDIX B

Collection locations for 84 upper to middle ERZ samples.

Pu‘u ‘Ō‘ō episode	Sample	Latitude	Longitude
Pre-Pu‘u ‘Ō‘ō			
	KE1922-09	19.378	-155.141
	KE1922-08	19.378	-155.141
	KE1963-14	19.375	-155.148
	KE1963-04	19.379	-155.138
	KE1963-03	19.379	-155.137
	KE1963-02	19.379	-155.137
	KE1965-20	19.145	-155.379
	KE1965-34	19.373	-155.157
	KE1965-15	19.376	-155.148
	KE1965-16	19.376	-155.147
	KE1965-17	19.376	-155.147
	KE1965-18	19.378	-155.141
	KE1965-19	19.380	-155.134
	KE1968-35	19.374	-155.158
	KE1968-36	19.375	-155.155
	KE1968-37	19.375	-155.152
	KE1968-10	19.377	-155.143
	KE1968-05	19.379	-155.140
	KE1968-07	19.379	-155.140
	KE1968-06	19.379	-155.139
	KE1968-23	19.380	-155.132
	KE1968-31	19.382	-155.131
	DAS69-3-2*	19.365	-155.216
	KI-77-13*	19.411	-155.074
	KI-77-11*	19.411	-155.072
Pu‘u ‘Ō‘ō - Episode 1			
	KE1983-13	19.378	-155.146
	KE1983-12	19.379	-155.145
	KE1983-11	19.379	-155.145
	KE1-49	19.378	-155.145
	KE1983-32	19.379	-155.132
	KE1-53	19.381	-155.129
	KE1983-30	19.380	-155.129
	KE1983-29	19.381	-155.127
	KE1983-27	19.383	-155.123
	KE1-5	19.385	-155.116
	KE1-58	19.390	-155.103
	KE1-37	19.396	-155.096
	KE1-38	19.398	-155.095
	KE1-25	19.395	-155.090
Pu‘u ‘Ō‘ō - Episode 35			
	KE35-389	19.389	-155.105
	KE35-390	19.389	-155.105
	KE35-394	19.389	-155.105

	KE35-396	19.396	-155.114
	KE35-397	19.386	-155.111
	KE35-399	19.385	-155.112
	KE35-404	19.382	-155.118
	KE35-408	19.384	-155.111
	KE35.410	19.387	-155.112
	KE35-412	19.386	-155.110
	KE35-413	19.388	-155.111
	KE35-414	19.388	-155.111
	KE35-419	19.386	-155.110
	KE35-421	19.386	-155.111
	KE35-425	19.386	-155.112
	KE35-438	19.387	-155.110
	KE35-439	19.387	-155.110
	KE35-441	19.386	-155.110
Pu‘u ‘Ō‘ō - Episode 54			
	Vent F*	19.372	-155.147
	Vent A*	19.374	-155.142
	Vent B*	19.376	-155.140
	Vent D*	19.377	-155.136
	Vent E*	19.379	-155.129
Pu‘u ‘Ō‘ō - Episode 59			
	KE59-2955	19.376	-155.137
	KE59-2958	19.376	-155.137
	KE59-2968	19.375	-155.137
	KE59-2980	19.375	-155.137
	KE59-2979	19.377	-155.135
	KE59-2942	19.378	-155.133
	KE59-2965	19.378	-155.133
	KE2011-33	19.378	-155.132
	KE59-2957	19.376	-155.132
	KE59-2964	19.378	-155.131
	KE59-2975	19.378	-155.130
	KE59-2952	19.380	-155.126
	KE59-2950	19.381	-155.125
	KE59-2974	19.380	-155.125
	KE59-2949	19.381	-155.124
	KE59-2947	19.382	-155.123
	KE59-2944	19.383	-155.122
	KE59-2960	19.383	-155.122
	KE59-2943	19.383	-155.121
	KE59-2959	19.384	-155.121
	KE59-2982	19.383	-155.121
	KE59-2972	19.384	-155.119

Notes: * Denote samples for which the location is inferred from a published map of the associated eruption. Episode 35 locations are from Thornber *et al.* (2002); episodes 58 and 60 locations are from M. Garcia (unpublished data). For each year or episode, samples are listed in in order of collection location from west to east. Samples from episodes 58 and 60 were collected from flows fed by Pu‘u ‘Ō‘ō.

APPENDIX C

Electron microprobe analyses (in wt. %) of olivine crystal cores.

Sample	SiO_2	FeO	MgO	NiO	CaO	Total	Fo%
Episode 54							
Vent A	39.56	16.41	43.53	0.22	0.27	99.98	82.5
	39.42	16.58	43.32	0.21	0.26	99.80	82.3
	39.46	16.79	43.13	0.21	0.26	99.85	82.1
	39.55	17.13	43.01	0.21	0.28	100.18	81.7
	39.52	17.22	42.76	0.21	0.28	99.99	81.6
	39.30	17.22	42.72	0.21	0.27	99.72	81.6
Episode 58							
24-Aug-07	38.71	17.36	42.62	0.18	0.24	99.34	81.4
	38.76	18.14	41.90	0.17	0.26	99.45	80.5
	39.29	18.82	41.26	0.17	0.25	100.02	79.6
23-Sep-08	39.09	17.34	42.44	0.20	0.23	99.53	81.4
	38.99	17.41	42.43	0.18	0.25	99.50	81.3
	39.46	17.75	42.27	0.18	0.24	100.13	80.9
	39.31	17.92	42.12	0.18	0.25	100.02	80.7
5-Apr-09	39.68	15.99	43.53	0.24	0.22	99.87	82.9
	39.46	17.03	42.63	0.21	0.23	99.79	81.7
	39.20	17.66	42.21	0.18	0.25	99.74	81.0
	39.32	17.65	42.27	0.18	0.25	99.90	81.0
	39.39	17.99	41.96	0.17	0.26	100.00	80.6
	39.45	17.94	41.41	0.19	0.21	99.42	80.5
	39.68	18.04	41.40	0.17	0.27	99.79	80.4
	39.34	19.27	39.97	0.15	0.30	99.27	78.7
6-Mar-10	39.45	17.94	41.41	0.19	0.21	99.42	80.5
	39.68	18.04	41.40	0.17	0.27	99.79	80.4
	39.74	18.03	41.59	0.18	0.25	100.01	80.4
	39.56	18.02	41.34	0.17	0.25	99.58	80.4
	39.71	18.14	41.47	0.18	0.25	99.98	80.3
	39.72	18.25	41.26	0.17	0.26	99.91	80.1
	39.48	18.39	41.11	0.17	0.26	99.65	79.9
	39.34	19.27	39.97	0.15	0.30	99.27	78.7
	39.45	17.94	41.41	0.19	0.21	99.42	80.5
12-Jan-11	38.81	18.60	41.67	0.17	0.25	99.74	80.0
	38.71	18.61	41.54	0.17	0.25	99.52	79.9
	38.81	18.68	41.55	0.17	0.25	99.70	79.9
	38.86	18.64	41.55	0.17	0.25	99.71	79.9
	39.05	18.68	41.72	0.17	0.25	100.1	79.9
	38.55	18.66	41.41	0.17	0.25	99.28	79.8
	38.74	18.70	41.45	0.17	0.26	99.57	79.8
	38.44	19.87	40.31	0.15	0.29	99.33	78.3
	38.81	18.60	41.67	0.17	0.25	99.74	80.0
Episode 59							
KE59-2955	39.48	17.02	42.94	0.19	0.25	99.88	81.8
	39.25	17.15	42.88	0.19	0.25	99.72	81.7
	39.40	17.38	42.59	0.20	0.25	99.82	81.4
	39.32	17.39	42.69	0.19	0.25	99.85	81.4
	38.59	20.23	40.29	0.16	0.28	99.54	78.0
	38.64	20.32	40.13	0.15	0.27	99.52	77.9
	38.22	20.48	40.25	0.16	0.25	99.34	77.8
	38.57	20.42	40.01	0.16	0.25	99.42	77.7
	38.51	20.62	40.39	0.14	0.27	99.92	77.7

	38.57	20.84	39.74	0.14	0.29	99.58	77.3
	38.58	20.80	39.82	0.15	0.25	99.61	77.3
	38.61	20.76	39.74	0.14	0.27	99.52	77.3
	38.42	21.33	39.26	0.14	0.28	99.43	76.6
	38.36	21.43	39.11	0.14	0.29	99.33	76.5
	38.30	22.27	38.83	0.14	0.30	99.83	75.7
KE59-2975	38.92	20.14	40.58	0.19	0.24	100.06	78.2
	38.69	20.22	40.39	0.18	0.24	99.71	78.1
	38.77	20.24	40.31	0.18	0.23	99.73	78.0
	38.63	20.48	40.02	0.17	0.26	99.56	77.7
	38.65	20.81	39.84	0.18	0.26	99.74	77.3
	38.48	21.03	39.42	0.16	0.25	99.34	77.0
	38.43	21.00	39.54	0.18	0.23	99.38	77.0
	38.17	21.43	39.38	0.16	0.25	99.39	76.6
	38.56	21.75	38.97	0.16	0.28	99.72	76.2
KE59-2980	38.74	19.04	41.24	0.15	0.25	99.44	79.4
	38.55	20.50	40.14	0.17	0.24	99.61	77.7
	38.50	20.97	39.56	0.15	0.28	99.46	77.1
	38.59	20.94	39.55	0.15	0.30	99.52	77.1
	38.58	21.09	39.55	0.14	0.29	99.66	77.0
	37.96	23.82	37.25	0.14	0.26	99.44	73.6
KE59-2982	38.75	20.24	40.38	0.18	0.23	99.77	78.1
	38.59	21.25	39.56	0.16	0.25	99.81	76.8
	38.95	20.48	37.81	0.15	2.18	99.58	76.7
	38.49	21.71	39.13	0.16	0.26	99.74	76.3
	38.31	21.81	39.00	0.15	0.28	99.55	76.1
	38.48	21.90	39.00	0.16	0.26	99.78	76.0
	38.25	22.17	38.69	0.17	0.26	99.52	75.7
	38.15	22.57	38.30	0.14	0.28	99.44	75.2
	38.22	22.46	38.28	0.14	0.28	99.39	75.2
	38.37	22.72	38.49	0.15	0.29	100.01	75.1
	38.10	23.18	37.79	0.14	0.27	99.48	74.4
Episode 61							
20-Jun-12	38.15	19.40	40.79	0.16	0.25	99.01	78.9
	38.84	19.46	40.76	0.16	0.24	99.72	78.9
	38.16	19.52	40.86	0.17	0.23	99.19	78.9
	38.37	19.46	40.85	0.17	0.24	99.34	78.9
	38.38	19.48	40.93	0.16	0.24	99.45	78.9
	38.25	19.51	40.71	0.16	0.25	99.13	78.8
	38.28	19.52	40.78	0.16	0.24	99.24	78.8
	38.51	19.56	40.65	0.16	0.24	99.39	78.7

Notes: Fo (forsterite) calculated as [Mg/(Mg+Fe)]*100 and Fo + Fa = 100 where Fa = fayalite component. Episode 58 data are from Lynn *et al.* (2017) and Lynn *et al.* (unpublished data). Episode 61 data are from Lynn *et al.* (unpublished data).

APPENDIX D

Glass major oxide compositions (in wt. %) for Nāpau Crater area samples.

Sample	SiO_2	TiO_2	Al_2O_3	FeO	MnO	MgO	CaO	Na_2O	K_2O	P_2O_5	Total	T [°C]
Pre-Puʻu ʻŌʻō												
KE1922-09	52.22	4.15	12.88	13.21	0.17	4.88	9.08	2.37	0.85	0.43	100.24	1119
KE1922-08	50.96	2.75	14.02	11.21	0.18	6.52	10.86	2.36	0.55	0.25	99.67	1148
KE1963-14	51.10	2.79	13.81	10.69	0.15	6.79	11.27	2.36	0.56	0.28	99.80	1155
KE1963-04	51.16	2.67	13.69	10.84	0.15	7.16	11.23	2.34	0.56	0.28	100.07	1154
KE1963-03	51.41	2.74	13.75	10.76	0.17	7.08	11.31	2.29	0.56	0.28	100.33	1156
KE1963-02	51.51	2.81	14.20	11.07	0.15	6.44	10.94	2.48	0.59	0.28	100.47	1150
KE1965-20	51.03	2.75	13.67	10.79	0.17	6.90	11.20	2.33	0.57	0.26	99.66	1154
KE1965-34	51.12	2.72	13.53	10.89	0.18	7.08	11.19	2.41	0.56	0.24	99.92	1154
KE1965-15	50.72	2.68	13.51	10.74	0.16	7.18	11.26	2.36	0.57	0.26	99.43	1155
KE1965-16	50.78	2.70	13.66	10.88	0.16	7.03	11.30	2.33	0.56	0.29	99.68	1156
KE1965-17	50.95	2.74	13.88	10.86	0.17	6.89	11.32	2.37	0.57	0.27	100.01	1156
KE1965-18	51.39	2.76	13.68	11.02	0.16	6.95	11.19	2.43	0.57	0.26	100.40	1154
KE1965-19	51.42	2.75	13.75	10.77	0.16	7.10	11.20	2.36	0.56	0.23	100.32	1154
KE1968-35	51.25	2.79	13.96	11.24	0.16	6.53	11.02	2.44	0.56	0.26	100.20	1151
KE1968-36	51.43	2.84	13.89	11.28	0.17	6.46	11.00	2.37	0.59	0.29	100.31	1151
KE1968-37	50.76	2.81	13.94	11.23	0.16	6.49	11.00	2.41	0.57	0.28	99.66	1151
KE1968-10	51.23	2.89	13.75	11.26	0.16	6.48	10.98	2.38	0.58	0.28	100.00	1150
KE1968-05	51.47	3.01	13.62	11.59	0.17	6.34	10.86	2.47	0.61	0.29	100.42	1148
KE1968-07	51.33	2.88	13.69	11.25	0.17	6.40	11.01	2.40	0.58	0.28	99.99	1151
KE1968-06	51.30	2.84	13.76	11.15	0.18	6.65	11.06	2.47	0.58	0.26	100.24	1152
KE1968-23	51.31	2.92	13.76	11.44	0.18	6.34	10.99	2.33	0.59	0.28	100.14	1150
KE1968-31	51.45	3.05	13.72	11.69	0.17	6.14	10.75	2.37	0.61	0.29	100.24	1146
Puʻu ʻŌʻō - Episode 1												
KE1983-13	50.94	2.83	13.83	11.33	0.16	6.24	10.68	2.31	0.54	0.26	99.11	1145
KE1983-12	51.18	3.11	13.38	12.19	0.17	6.02	10.40	2.36	0.60	0.31	99.72	1141
KE1983-11	51.07	2.84	13.82	11.38	0.18	6.34	10.72	2.40	0.54	0.27	99.55	1146
KE1983-32	51.18	3.26	13.42	12.07	0.19	5.76	10.24	2.53	0.63	0.33	99.61	1138
KE1983-30	51.12	3.24	13.39	11.91	0.17	5.90	10.39	2.41	0.62	0.35	99.51	1140
KE1983-29	50.82	3.23	13.39	12.04	0.20	5.90	10.37	2.43	0.64	0.33	99.35	1140
KE1983-27	51.03	3.11	13.66	11.83	0.17	6.01	10.48	2.47	0.61	0.29	99.66	1142
Puʻu ʻŌʻō - Episode 54												
Vent F	51.66	3.72	13.44	12.28	0.17	5.31	9.63	2.65	0.76	0.40	100.02	1128
Vent A	51.33	3.03	13.91	11.59	0.18	6.27	10.64	2.36	0.59	0.30	100.19	1145
Vent B	51.13	3.25	13.55	11.91	0.18	6.07	10.40	2.54	0.63	0.32	99.98	1141
Vent D	51.21	3.08	13.73	11.49	0.17	6.33	10.48	2.44	0.60	0.28	99.82	1142
Puʻu ʻŌʻō - Episode 59												
KE59-2955	51.75	2.92	13.56	11.80	0.18	6.15	10.42	2.40	0.52	0.26	99.93	1141
KE59-2958	51.42	3.03	13.36	12.07	0.18	6.17	10.23	2.42	0.56	0.28	99.84	1138
KE59-2968	51.54	3.06	13.41	12.07	0.18	6.19	10.30	2.43	0.54	0.28	100.12	1139
KE59-2980	51.54	3.31	13.06	12.73	0.19	5.72	9.92	2.45	0.62	0.30	99.95	1133
KE59-2979	51.23	3.09	13.77	11.75	0.18	5.94	10.16	2.50	0.61	0.30	99.53	1137
KE59-2942	51.13	3.19	13.56	11.85	0.17	5.97	10.18	2.49	0.61	0.29	99.45	1137
KE59-2965	51.30	3.12	13.60	11.85	0.16	6.07	10.23	2.54	0.61	0.30	99.78	1138
KE2011-33	51.10	3.04	13.70	11.79	0.18	6.08	10.34	2.46	0.59	0.30	99.58	1140
KE59-2957	51.60	2.91	13.38	11.83	0.17	6.08	10.36	2.37	0.52	0.26	99.47	1140
KE59-2964	51.14	3.22	13.37	11.97	0.18	5.86	10.14	2.48	0.62	0.31	99.29	1136
KE59-2952	51.34	3.10	13.59	11.75	0.19	6.14	10.37	2.52	0.61	0.33	99.94	1140
KE59-2950	51.38	3.09	13.62	11.68	0.17	6.14	10.29	2.49	0.61	0.30	99.76	1139
KE59-2974	51.24	3.23	13.41	12.10	0.18	6.02	10.17	2.42	0.64	0.32	99.74	1137
KE59-2949	51.27	3.15	13.59	11.77	0.17	6.04	10.21	2.51	0.63	0.31	99.64	1137

KE59-2947	51.28	3.19	13.63	11.81	0.17	6.05	10.12	2.53	0.63	0.31	99.72	1136
KE59-2944	51.28	3.23	13.63	11.93	0.17	5.75	10.03	2.55	0.64	0.31	99.52	1134
KE59-2960	51.58	3.30	13.35	12.06	0.18	5.78	9.98	2.51	0.65	0.34	99.73	1134
KE59-2943	51.07	3.34	13.15	12.28	0.18	5.69	9.98	2.46	0.64	0.33	99.13	1134
KE59-2959	51.15	3.45	13.20	12.59	0.19	5.66	9.72	2.56	0.68	0.33	99.66	1129
KE59-2982	51.35	3.28	13.43	12.13	0.18	5.93	10.00	2.58	0.65	0.33	99.99	1134
KE59-2972	51.52	3.01	13.29	12.10	0.17	6.04	10.27	2.43	0.54	0.27	99.64	1139

Notes: Column ‘T °C’ lists sample eruption temperature (uncertainty of ±8-10 °C) based on CaO geothermometer developed for Kīlauea ERZ glass compositions by Helz & Thornber (1987). See Appendix B for sample locations.

APPENDIX E

Input parameters and timescale results for episode 59 olivine.

Natural Data	Boundary & Initial Conditions				Numerical Scheme		Best Fit			
Sample	T (°C)	C (x, t=0)	C (Xmin, t)	C (Xmax, t)	Xmax (μm)	Dx (μm)	Discrepancy (%)	Time (hours)	Error (-days)	Error (+days)
KE59-2955-ol3.2	1141	0.765	0.790	0.765	18	1	38	6	2	2
KE59-2975-ol3	1138	0.770	0.774	0.770	32	2	0	28	11	41
KE59-2982-ol5.1	1134	0.743	0.765	0.743	32	2	0	102	18	20
KE59-2982-ol8	1134	0.756	0.766	0.756	30	2	15	51	10	11
Average								47	10	18

Notes: Calculated using DIPRA (Girona & Costa, 2013). Only the reversely zoned portion of each profile was modeled. Xmax is the total distance in microns of the modeled profile and Dx is the spacing between data points of said profile. Discrepancy is the percentage of data points in the calculated best-fit profile that fall outside of an error of 0.1 % Fo. Initial conditions appropriate for Kīlauea include the following for each model: Pressure, 0.5 GPa; Fo uncertainty, 0.001%; Temperature, 'T (°C)', lists sample eruption temperature (uncertainty of ±8-10 °C) based on Cao-based geothermometer developed for Kīlauea ERZ glass compositions by Helz & Thornber (1987), no glass composition was available for sample KE59-2975, so a whole-rock CaO composition was used as a proxy; Oxygen fugacity, NNO-0.72 (log fO2 ranged from -8.97 to -9.06), Helz *et al.* (2017).

APPENDIX F

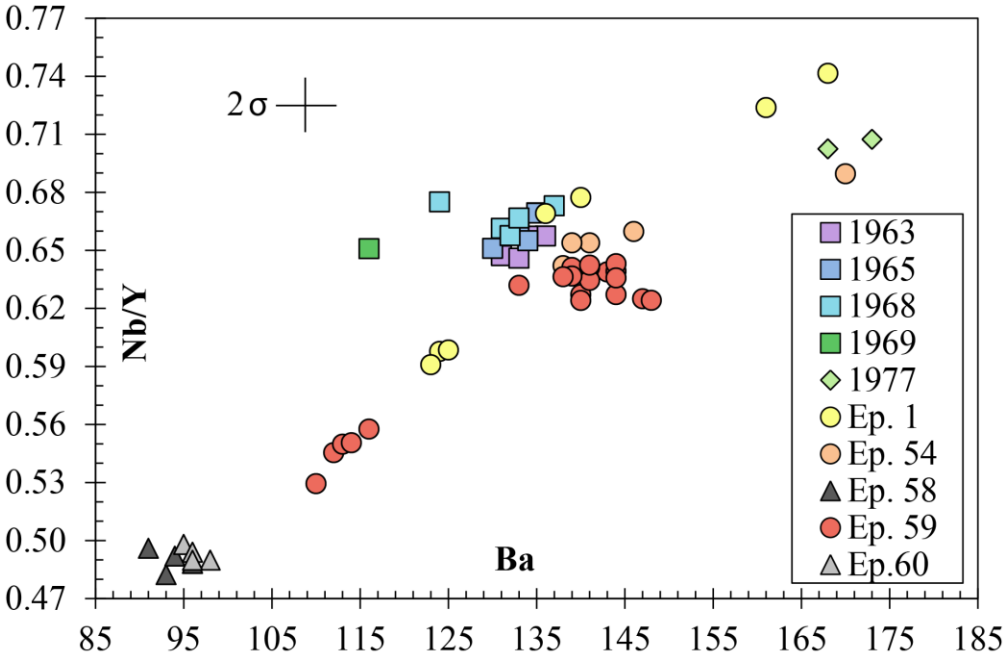

Nb/Y vs. Ba variation from upper to middle ERZ lavas. Nb concentrations were normalized by Y to remove the effect of any olivine, clinopyroxene, and/or plagioclase fractionation on parental magma compositions. Data for samples DAS69-3-2 and KI-77-11 are from Pietruszka *et al.* (in preparation). Data for episodes 58 and 60 are from M. Garcia (unpublished data). See Appendix B for sample locations.

REFERENCES CITED

Armstrong, J. T. (1988). Quantitative analysis of silicates and oxide minerals: Comparison of Monte-Carlo, ZAF and Phi-Rho-Z procedures. In: Newbury, D.E. (ed.) *Microbeam Analysis*. San Francisco Press USA.

Baker, S. & Amelung, F. (2015). Pressurized magma reservoir within the east rift zone of Kīlauea Volcano, Hawai‘i: Evidence for relaxed stress changes from the 1975 Kalapana earthquake. *Geophysical Research Letters* **42**, 1758-1765.

Carr, M. J. & Gazel, E. (2017). Igpet software for modeling igneous processes: Examples of application using the open educational version. *Mineralogy and Petrology* **111**, 283-289.

Clauge, D. A., Moore, J. G., Dixon, J. E. & Friesen, W. B. (1995). Petrology of submarine lavas from Kilaueas Puna Ridge, Hawaii. *Journal of Petrology* **36**, 229-349.

Danyushevsky, L. V. & Plechov, P. (2011). Petrolog3: Integrated software for modeling crystallization processes. *Geochemistry, Geophysics, Geosystems* **12**.

Dohmen, R. & Chakraborty, S. (2007). Fe-Mg diffusion in olivine II: point defect chemistry, change of diffusion mechanisms and a model for calculation of diffusion coefficients in natural olivine. *Physics and Chemistry of Minerals* **34**, 409-430.

Dzurisin, D., Koyanagi, R. Y. & English, T. T. (1984). Magma supply and storage at Kilauea Volcano, Hawaii, 1956-1983. *Journal of Volcanology and Geothermal Research* **21**, 177-206.

Folk, R. L. (1968). *Petrology of Sedimentary Rocks*. Hemphill’s Austin, TX USA.

Garcia, M. O., Ho, R. A., Rhodes, J. M. & Wolfe, E. W. (1989). Petrologic constraints on rift-zone processes: Results from episode 1 of the Puu Oo eruption of Kilauea volcano, Hawaii. *Bulletin of Volcanology* **52**, 81-96.

Garcia, M. O., Pietruszka, A. J., Rhodes, J. M. & Swanson, K. (2000). Magmatic processes during the prolonged Pu’u’O’o eruption of Kilauea Volcano, Hawaii. *Journal of Petrology **41***, 967-990.

Garcia, M. O., Rhodes, J. M., Wolfe, E. W., Ulrich, G. E. & Ho, R. A. (1992). Petrology of lavas from episodes 2-47 of the Puu Oo eruption of Kilauea Volcano, Hawaii: evaluation of magmatic processes. Bulletin of Volcanology 55, 1-16.

Girona, T. & Costa, F. (2013). DIPRA: A user-friendly program to model multi-element diffusion in olivine with applications to timescales of magmatic processes. *Geochemistry, Geophysics, Geosystems* **14**, 422-431.

Harris, A. J. L., Keszthelyi, L., Flynn, L. P., Mouginis-Mark, P. J., Thornber, C., Kauahikaua, J., Sherrod, D., Trusdell, F., Sawyer, M. W. & Flament, P. (1997). Chronology of the episode 54 eruption at Kilauea Volcano, Hawaii, from GOES-9 satellite data. *Geophysical Research Letters* **24**, 3281-284.

Heliker, C. & Mattox, T. N. (2003). *The first two decades of the Pu'u 'Ō'ō-Kūpaianaha eruption: Chronology and selected bibliography*. In: Heliker, C., Swanson, D.A., Takahashi, T.J. (eds.) *The Pu'u 'Ō'ō-Kūpaianaha eruption of Kīlauea Volcano, Hawai'i: The First 20 Years*. *U. S. Geological Survey Professional Paper* **1676**, 1-27.

Helz, R. T. & Thornber, C. R. (1987). Geothermometry of Kilauea Iki lava lake, Hawaii. *Bulletin of Volcanology* **49**, 651-668.

Helz, R. T., Cottrell, E., Brounce, M. N. & Kelley, K. A. (2017). Olivine-melt relationships and syneruptive redox variations in the 1959 eruption of Kīlauea Volcano as revealed by XANES. *Journal of Volcanology and Geothermal Research* **333**, 1-14.

Henderson, P. (1982). *Inorganic Chemistry*. Pergamon Press UK.

Hoffmann, J. P., Ulrich, G. E. & Garcia, M. O. (1990). Horizontal ground deformation patterns and magma storage during the Puu Oo eruption of Kilauea volcano, Hawaii: episodes 22-42. *Bulletin of Volcanology* **52**, 522-531.

Jackson, D. B., Swanson, D. A., Koyanagi, R. Y. & Wright, T. L. (1975). The August and October 1968 east rift eruptions of Kilauea Volcano, Hawaii. *U. S. Geological Survey Professional Paper* **890**, 1-33.

Jaggar, T. A. (1922). *Monthly Bulletin of the Hawaiian Volcano Observatory: May 1922*. In: Bevens, D., Takahashi, T. J. & Wright, T. L. (eds.) 1988. *The early serial publications of the Hawaiian Volcano Observatory **3**. Monthly bulletin of the Hawaiian Volcano Observatory (1921-1929).* Hawaii Natural History Association USA.

Jarosewich, E., Nelen, J. A. & Norberg, J. A. (1980). Reference samples for electron microprobe analysis. *Geostandards and Geoanalytical Research **4***, 43-47.

Klein, F. W., Koyanagi, R. Y., Nakata, J. S. & Tanigawa, W. R. (1987). *The seismicity of Kilauea's magma system.* In: Decker R. W., Wright T. L. & Stauffer P. H. (eds.) *Volcanism in Hawaii **2**. U. S. Geological Survey Professional Paper 1350*, 1019-1185.

Lundgren, P., Poland, M., Miklius, A., Orr, T., Yun, S. H., Fielding, E., Liu, Z., Tanaka, A., Szeliga, W., Hensley, S. & Owen, S. (2013). Evolution of dike opening during the March 2011 Kamoamoa fissure eruption, Kīlauea Volcano, Hawaii. *Journal of Geophysical Research: Solid Earth* **118**, 897-914.

Lynn, K. J., Shea, T. & Garcia, M. O. (2017). Nickel variability in Hawaiian olivine: Evaluating the relative contributions from mantle and crustal processes. *American Mineralogist* **102**, 507-518.

Macdonald, G. A., Abbott, A. T. & Peterson, F. L. (1983). *Volcanoes in the sea: The Geology of Hawaii.* University of Hawaii Press USA.

Matzen, A. K., Baker, M. B., Beckett, J. R. & Stolper, E. M. (2011). Fe-Mg partitioning between olivine and high-magnesian melts and the nature of Hawaiian parental liquids. *Journal of Petrology* **52**, 1243-1263.

Mittelstaedt, E. & Garcia, M. O. (2007). Modeling the sharp compositional interface in the Pu‘u ‘Ō‘ō magma reservoir, Kīlauea volcano, Hawai‘i. *Geochemistry, Geophysics, Geosystems* **8**, 1-13.

Moore, J. G. & Ault, W. U. (1965). Historic littoral cones in Hawaii. *Pacific Science* **19**, 3-11.

Moore, J.G. & Koyanagi, R.Y. (1969). The October 1963 eruption of Kilauea Volcano, Hawaii. *U. S. Geological Survey Professional Paper* **614-C**, 1-13.

Moore, R. B., Helz, R. T., Dzurisin, D., Eaton, G. P., Koyanagi, R. Y., Lipman, P. W., Lockwood, J.P. & Puniwai, G. S. (1980). The 1977 eruption of Kilauea volcano, Hawaii. *Journal of Volcanology and Geothermal Research* **7**, 189-210. of/2007/1089/.

Okamura, A. T., Dvorak, J. J., Koyanagi, R. Y. & Tanagawa W. J. L. (1988). *Surface deformation during dike propagation*. In: Wolfe, E. W. (ed.) *The Pu‘u ‘Ō‘ō eruption of Kilauea Volcano, episodes 1-20 January 3, 1983, to June 8*, 1984. *U. S. Geological Survey Professional Paper **1463***, 165-181.

Orr, T. R., Poland, M. P., Patrick, M. R., Thelen, W. A., Sutton, A. J., Elias, T., Thornber, C. R., Parcheta, C. & Wooten, K. M. (2015). *Kīlauea's 5-9 March 2011 Kamoamoa Fissure*

Eruption and Its Relation to 30 Years of Activity From Pu‘u ‘Ō ‘ō. In: Carey, R., Cayol, V., Poland, M., Weis, D. (eds.) *Hawaiian Volcanoes from Source to Surface Geophysical Monograph Series **208***, 393-420.

Owen, S., Segall, P., Lisowski, M., Miklius, A., Murray, M., Bevis, M. & Foster, J. (2000). January 30, 1997 eruptive event on Kilauea Volcano, Hawaii, as monitored by continuous GPS. *Geophysical Research Letters* **27**, 2757-2760.

Pearce, T. H. (1984). The analysis of zoning in magmatic crystals with emphasis on olivine. *Contributions to Mineralogy and Petrology* **86**, 149-154.

Poland, M. P., Miklius, A., Sutton, A. J. & Thornber, C. R. (2012). A mantle-driven surge in magma supply to Kīlauea Volcano during 2003-2007, *Nature Geoscience* **5**, 295-300.

Rhodes, J. M. & Vollinger, M. J. (2004). Composition of basaltic lavas sampled by phase-2 of the Hawaii Scientific Drilling Project: Geochemical stratigraphy and magma types. *Geochemistry, Geophysics, Geosystems* **5**, 1-38.

Rhodes, J. M., & Vollinger, M. J. (2005). Ferric/ferrous ratios in 1984 Mauna Loa lavas: a contribution to understanding the oxidation state of Hawaiian magmas. *Contributions to Mineralogy and Petrology* **149**, 666-674.

Richter, D. H., Ault, W. U., Eaton, J.P. & Moore, J. G. (1964). The 1961 eruption of Kilauea Volcano, Hawaii. *U. S. Geological Survey Professional Paper* **474-D**, 1-34.

Roeder, P. L. & Emslie, R. F. (1970). Olivine-liquid equilibrium. *Contributions to Mineralogy and Petrology* **29**, 275-289.

Sherrod, D. R., Sinton, J. M., Watkins, S. E., & Brunt, K. M. (2007). Geologic map of the State of Hawaii. *U. S. Geological Survey, Open-File Report* **2007-1089**, http://pubs.usgs.gov/of/2007/1089/.

Siebert, L., Cottrell, E., Venzke, E. & Andrews, B. (2015). *Earth’s Volcanoes and Their Eruptions: An Overview.* In: Sigurdsson, H., Houghton, B., McNutt, S. R., Rymer, H. & Stix, J. (eds.) *The Encyclopedia of Volcanoes*. Elsevier.

Swanson, D. A., Jackson, D. B., Koyanagi, R. Y. & Wright, T. L. (1976). The February 1969 east rift eruption of Kilauea Volcano, Hawaii. *U. S. Geological Survey Professional Paper* **891**, 1-30.

Thornber, C. R., Heliker, C., Sherrod, D. R., Kauahikaua, J. P., Miklius, A., Okubo, P. G., Trusdell, F. A., Budahn, J. R., Ridley, W. I. & Meeker, G. P. (2003). Kilauea east rift zone magmatism: An episode 54 perspective. *Journal of Petrology* **44**, 1525-1559.

Thornber, C. R., Orr, T. R., Heliker, C. & Hoblitt, R. P. (2015). Petrologic testament to changes in shallow magma storage and transport during 30+ years of recharge and eruption at Kīlauea Volcano, Hawai'i, In: Carey, R., Cayol, V., Poland, M., Weis, D. (eds.) *Hawaiian Volcanoes from Source to Surface Geophysical Monograph Series **208***, 147-188.

Thornber, C. R., Sherrod, D. R., Siems, D. F., Heliker, C. C., Meeker, G. P., Oscarson, R. L., & Kauahikaua, J. P. (2002). Whole-rock and glass major-element geochemistry of Kilauea Volcano, Hawaii, near-vent eruptive products: September 1994 through September 2001. *U. S. Geological Survey, Open-File Report* **2002-17**, https://pubs.usgs.gov/of/2002/0017/pdf/of02-017.pdf.

Tilling, R. I., & Dvorak, J. J. (1993). Anatomy of a basaltic volcano. *Nature* **363**, 125-133.

U. S. Geological Survey. (2000). US GeoData Digital Elevation Models. *U. S. Geological Survey, Open-File Report* **040-00**, https://pubs.er.usgs.gov/publication/fs04000

Wass, S. Y. (1973). The origin and petrogenetic significance of hour-glass zoning in titaniferous clinopyroxenes. *Mineralogical Magazine* **39**, 133-144.

Welsch, B., Hammer, J., Baronnet, A., Jacob, S., Hellebrand, E. & Sinton, J. (2016). Clinopyroxene in postshield Haleakala ankaramite: 2. Texture, compositional zoning and supersaturation in the magma. *Contributions to Mineralogy and Petrology* **171**, 1-19.

Wolfe E. W., Garcia, M. O., Jackson, D. B., Koyanagi, R. Y., Neal, C. A. & Okamura, A. T. (1987). *The Puu Oo eruption of Kilauea Volcano, episodes 1-20 January 3, 1983, to June 8, 1984.* In: Decker R. W., Wright T. L. & Stauffer P. H. (eds.) *Volcanism in Hawaii **1** U. S. Geological Survey Professional Paper **1350***, 471-508.

Wolfe, E. W., Neal, C. A., Banks, N. G., Duggan, T. J. (1988). *Geologic observations and chronology of eruptive events.* In: Wolfe, E. W. (ed.) *The Puu Oo eruption of Kilauea Volcano, episodes 1-20 January 3, 1983, to June 8, 1984. U. S. Geological Survey Professional Paper **1463***, 165-181.

Wright, T. L. & Fiske, R. S. (1971). Origin of the differentiated and hybrid lavas of Kilauea volcano, Hawaii. *Journal of Petrology **12***, 1-65.

Wright, T. L. & Helz, R. T. (1996). Differentiation and magma mixing on Kilauea's east rift zone: A further look at the eruptions of 1955 and 1960. Part II. The 1960 lavas. *Bulletin of Volcanology* **57**, 602-630.

Wright, T. L. & Okamura, R. T. (1977). Cooling and crystallization of tholeiitic basalt, 1965 Makaopuhi lava lake, Hawaii. *U. S. Geological Survey Professional Paper* **1004**, 1-75.

Wright, T. L. (1971). Chemistry of Kilauea and Mauna Loa lava in space and time. *U. S. Geological Survey Professional Paper* **735**, 1-40.

Wright, T. L., Kinoshita, W. T. & Peck, D. L. (1968). The March 1965 eruption of Kilauea Volcano, and the formation of Makaopuhi lava lake. *Journal of Geophysical Research* **73**, 3181-3205.